

Substrate and Product Binding inside a Stimuli-Responsive Coordination Cage acting as Singlet Oxygen Photosensitizer

Sonja Pullen,^{a,‡} Susanne Löffler,^{a,‡} André Platzek,^a Julian J. Holstein^a and Guido H. Clever^{a*}

^aFaculty of Chemistry and Chemical Biology, TU Dortmund University, Otto Hahn Str. 6, 44227 Dortmund, Germany

[‡]These authors contributed equally to this work.

Electronic Supplementary Information

General Methods.....	2
NMR.....	2
Single crystals X-ray structure determination	2
Mass spectrometry and ion mobility measurements.....	2
UV-Vis	2
Irradiation	2
Experimental Procedures	3
Synthesis of [3BF ₄ @Pd ₄ L ₈]	3
Anion exchange to form [2Cl@Pd ₄ L ₈]	4
Preparation of host-guest complex [C ₆ H ₈ @Pd ₄ L ₈]	5
Binding constant determination for [C ₆ H ₈ @Pd ₄ L ₈]	5
Preparation of [Pd ₂ L ₄]	7
Preparation of [Pd(terpy)CH ₃ CN].....	7
Preparation of [L(Pd-terpy) ₂]	8
Models of [L(Pd-terpy) ₂] and L.....	10
Further supporting figures and tables	11
Crystallographic Details	27
Measurement and processing details of [2Cl+C ₆ H ₈ O ₂ @Pd ₄ L ₈]	28
Specific refinement details of [2Cl+C ₆ H ₈ @Pd ₄ L ₈] and [2Cl+C ₆ H ₈ O ₂ @Pd ₄ L ₈]	28
References	31

General Methods

NMR

NMR spectroscopic data was measured on the spectrometers Bruker AV 500 Avance NEO, AV 600 Avance III HD, AV 700 Avance III HD. For ^1H and ^{13}C NMR spectra, chemical shifts were calibrated to the solvent lock signal. For ^{19}F NMR spectra, CFCl_3 (^{19}F , 0 ppm) were used as external standards. Chemical shifts δ are given in ppm, coupling constants J in Hz. All spectra were recorded in standard 5 mm NMR tubes at 25 °C, if not mentioned otherwise.

Single crystals X-ray structure determination

Bruker D8 venture diffractometer (in-house): Single crystal X-ray diffraction data was collected on a Bruker D8 venture equipped with an Incoatec microfocus source ($I_{\mu\text{s}}$ 3.0) using $\text{CuK}\alpha$ radiation on a four axis κ -goniometer, equipped with an Oxford Cryostream 800 device and a Photon II detector.

Synchrotron beamline P11@DESY: Single crystal X-ray diffraction data was collected at macromolecular beamline P11, Petra III, DESY (a member of the Helmholtz Association, HGF), Hamburg, Germany. Samples were mounted using the Stäubli TX60L robotic arm. A wavelength of $\lambda = 0.5636 \text{ \AA}$ was chosen using a liquid N_2 cooled double crystal monochromator. Single crystal X-ray diffraction data was collected at 80(2) K on a single axis goniometer, equipped with an Oxford Cryostream 800 device and a Pilatus 6M fast detector.

Mass spectrometry and ion mobility measurements

Mass spectrometry and trapped ion mobility data were measured on Bruker ESI-timsTOF (electrospray ionization-trapped ion mobility-time of flight) and Bruker compact high-resolution LC mass spectrometers (positive/negative mode). For calibration of the TIMS and TOF devices, Agilent ESI-Low Concentration Tuning Mix was used.

UV-Vis

UV vis spectra were recorded on a DAD HP-8453 UV-Vis spectrometer.

Irradiation

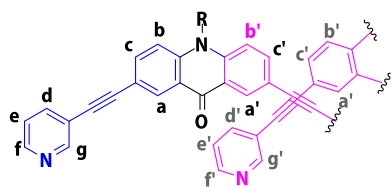
For irradiation experiments, a Merck photoreactor equipped with a 365 nm LED (3.4 W) was used. The light intensity was set to 100 % and ventilation was set to maximum power. Samples were irradiated for 40 minutes in 1 mL screw cap vials and the solution was then transferred to the NMR tube.

Experimental Procedures

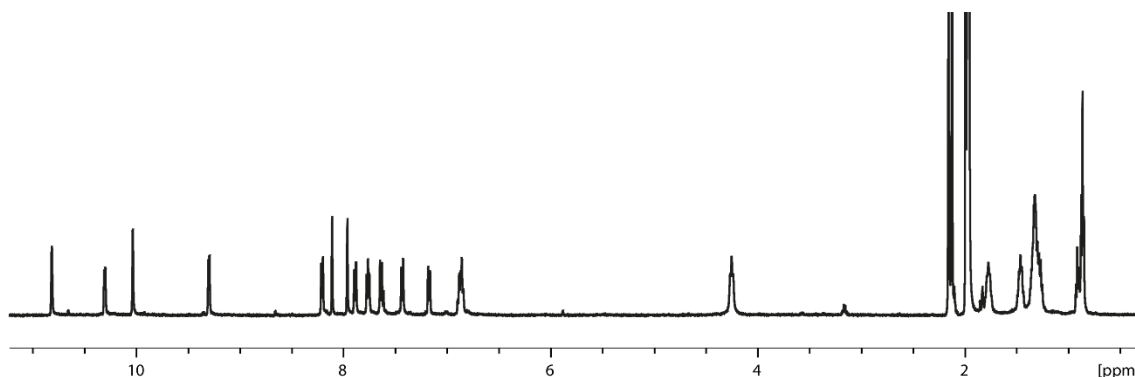
Where necessary, experiments were performed under nitrogen atmosphere using standard Schlenk techniques. Chemicals and standard solvents were purchased from Sigma Aldrich, Acros Organics, Carl Roth, TCI Europe, VWR, ABCR or other suppliers and used as received, if not mentioned differently. Dry solvents were purchased or purified and dried over absorbent-filled columns on a GS-Systems solvent purification system (SPS). Reactions were monitored with thin layer chromatography (TLC) using silica coated aluminium plates (Merck, silica 60, fluorescence indicator F254, thickness 0.25 mm). For column chromatography, silica (Merck, silica 60, 0.02–0.063 mesh ASTM) was used as the stationary phase, if not mentioned otherwise. Acridone ligand **L** was synthesized as reported previously.¹

Synthesis of [3BF₄@Pd₄L₈]

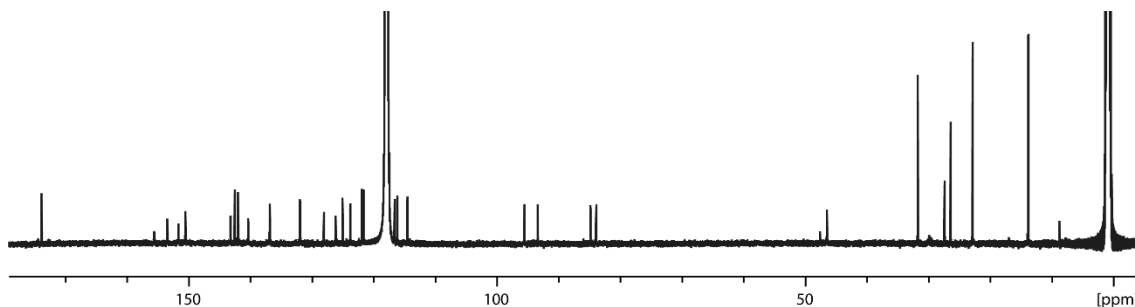
The interpenetrated coordination cages were prepared as reported earlier.¹ [3BF₄@Pd₄L₈] was obtained in quantitative yield by heating a mixture of ligand **L** (2.80 mM, 1.0 eq suspension in CD₃CN) and tetrakis(acetonitrile)palladium(II)-tetrafluoroborate (1.50 mM, 0.55 eq solution in CD₃CN) at 70 °C for 24 h.



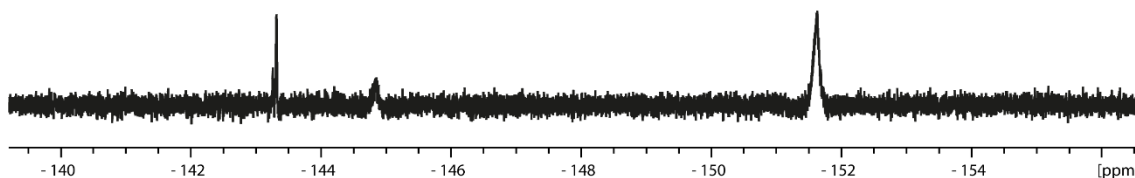
¹H NMR (500 MHz, 298 K, CD₃CN): δ (ppm) = 10.82 (s, 16H, g'), 10.29 (d, ³J = 5.25 Hz, 16H, f'), 10.03 (s (br), 16H, g), 9.29 (d, ³J = 5.95 Hz, 16H, f), 8.20 (d, ³J = 7.9 Hz, 16H, d), 8.11 (d, ³J = 2.0 Hz, 16H, a), 7.96 (d, ³J = 1.95 Hz, 16H, a'), 7.88 (dd, ³J = 8.7 Hz, ⁴J = 2.0 Hz, 16H, c), 7.76 (dt, ³J = 6.15 Hz, ⁴J = 1.3 Hz, 16H, e), 7.63 (d, ³J = 9.1 Hz, 16H, b), 7.43 (d, ³J = 9.0 Hz, 16H, b'), 7.17 (dd, ³J = 8.65 Hz, ⁴J = 1.9 Hz, 16H, c'), 6.85 (m, 32H, e', d'), 4.25 (t, ³J = 6.6 Hz, 16H, NCH₂), 1.77 (m, 16H, NCH₂CH₂), 1.47 - 1.25 (m, 48H, CH₂), 0.86 (t, ³J = 6.95 Hz, 24H, CH₃).



¹³C{¹H} NMR (176 MHz, 298 K, CD₃CN): δ = 173.8, 155.6, 153.4, 151.6, 150.5, 143.2, 142.5, 142.0, 140.3, 136.8, 131.9, 128.1, 126.2, 125.0, 123.8, 121.9, 121.6, 117.5, 116.6, 116.1, 114.5, 95.6, 93.4, 84.8, 83.9, 46.5, 31.8, 27.4, 26.4, 22.9, 13.8.



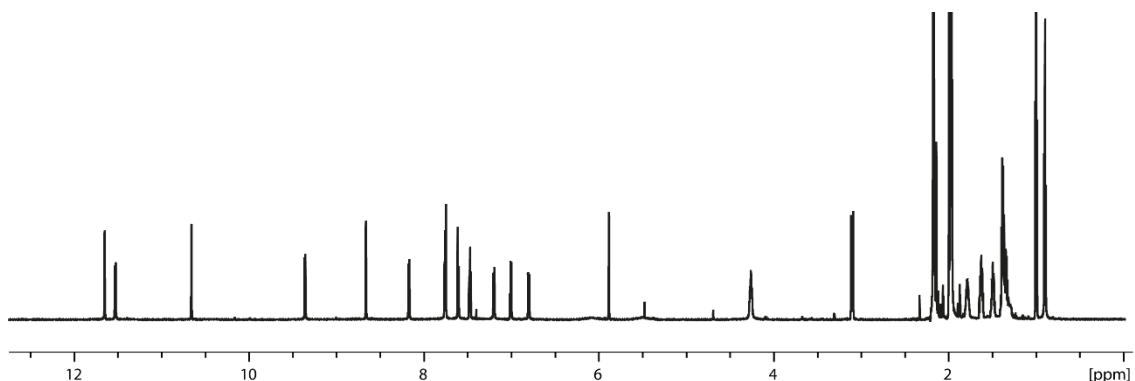
$^{19}\text{F}\{^1\text{H}\}$ NMR (471 MHz, 298 K, CD_3CN): $\delta = -143.3$ (s (br), $^1J(^{19}\text{F}-^{11}\text{B}) = 25.57$ Hz, 4F), -144.9 (s (br), 8F), -151.6 , (s (br), 20F).



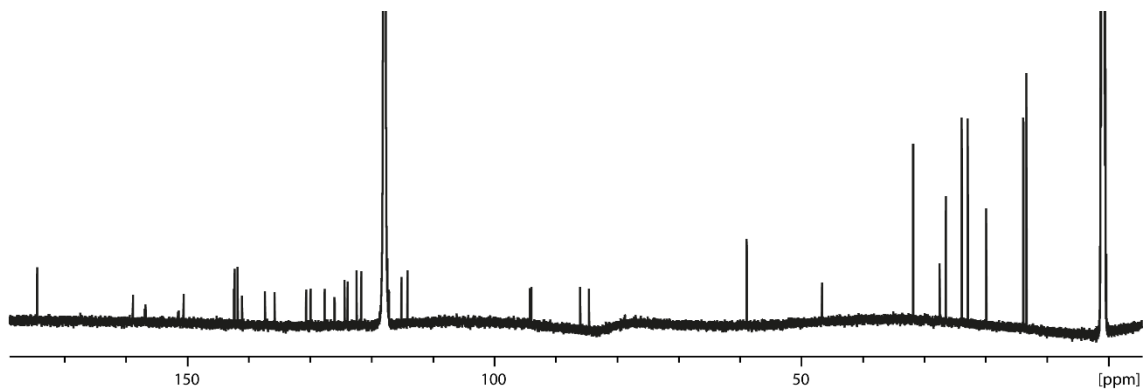
Anion exchange to form **[2Cl@Pd₄L₈]**

The chloride containing coordination cage **[2Cl@Pd₄L₈]** was formed by adding 20 μL (2 eq) of a solution of tetrabutylammonium chloride (in CD_3CN , 17.5 mM) to 500 μL of a solution of **[3BF₄@Pd₄L₈]** (in CD_3CN , 0.35 mM). The coordination cage forms rapidly in quantitative yield after briefly shaking of the NMR tube.

^1H NMR (700 MHz, 298 K, CD_3CN): δ (ppm) = 11.65 (s, 16H, g), 11.53 (d, $^3J = 5.6$ Hz, 16H, f'), 10.66 (s, 16H, g'), 9.36 (d, $^3J = 5.45$ Hz, 16H, f), 8.66 (s, 16H, a'), 8.17 (d, $^3J = 7.55$ Hz, 16H, d), 7.74 (m, 32H, c,e), 7.60 (d, $^3J = 8.5$ Hz, 16H, b), 7.47 (t, $^3J = 6.7$ Hz, 16H, e'), 7.19 (d, $^3J = 8.8$ Hz, 16H, b'), 7.00 (d, $^3J = 7.35$ Hz, 16H, d'), 6.80 (d, $^3J = 8.45$ Hz, 16H, c'), 5.88 (d, $^4J = 1.45$ Hz, 16H, a), 4.26 (t, $^3J = 8.55$ Hz, 16H, NCH₂), 1.78 (m, 16H, NCH₂CH₂), 1.49 (m, 16H, NCH₂CH₂CH₂), 1.35 (m, 32H, CH₂CH₂CH₃), 0.90 (t, $^3J = 7.21$ Hz, 24H, CH₃).



$^{13}\text{C}\{^1\text{H}\}$ NMR (176 MHz, 298 K, CD_3CN): 174.4, 158.8, 150.6, 142.3, 141.8, 141.1, 137.3, 135.8, 130.6, 129.9, 127.6, 126.0, 124.4, 123.9, 122.4, 121.7, 117.4, 115.1, 114.1, 94.2, 94.0, 86.0, 84.6, 58.9, 31.8, 26.5, 23.9, 22.9, 19.9, 13.9, 13.3.



Preparation of host-guest complex $[C_6H_8@Pd_4L_8]$

To a solution of $[2Cl@Pd_4L_8]$ (0.35 mM, CD_3CN) 30 eq. of a solution of **1** (CD_3CN , 70 mM) was added. The solution was allowed to equilibrate for 24 h. The equilibrium of this reaction lies strongly on the product $[C_6H_8@Pd_4L_8]$ site; only small amounts of free $[2Cl@Pd_4L_8]$ are still visible in the 1H -NMR spectrum after 24h.

Binding constant determination for $[C_6H_8@Pd_4L_8]$

The binding constant of host-guest complex $[C_6H_8@Pd_4L_8]$ was determined as described previously.¹ Three solutions of $[2Cl@Pd_4L_8]$ (0.35 mM in CD_3CN) were prepared. To these solutions, 20 eq., 30 eq. and 40 eq. of 1,3-cyclohexadiene (70 mM stock solution in CD_3CN) was added. Encapsulation was followed by 1H -NMR spectroscopy. After equilibration, for each case, the binding constant (K_a) was determined by integration of the signals for free host [H], free guest [G] and host-guest complex [HG].

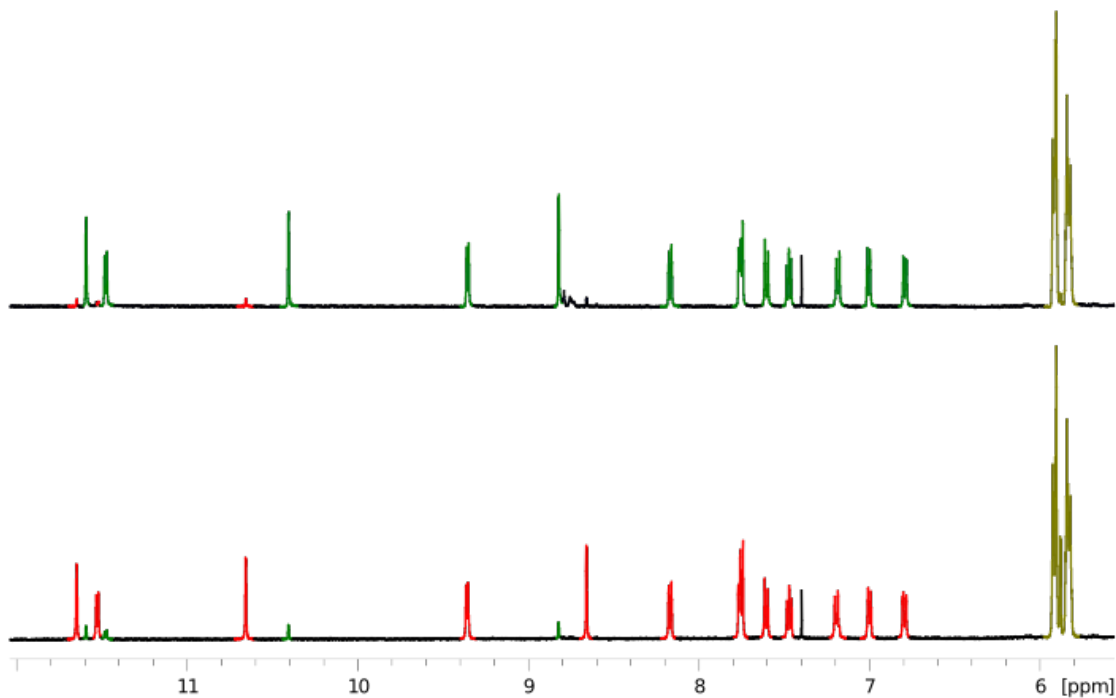
$$K_a = \frac{[HG]}{([H]_0 - [HG]) * ([G]_0 - [HG])}$$

Binding constant (20 eq.) = $2.19 \times 10^3 \text{ L mol}^{-1}$

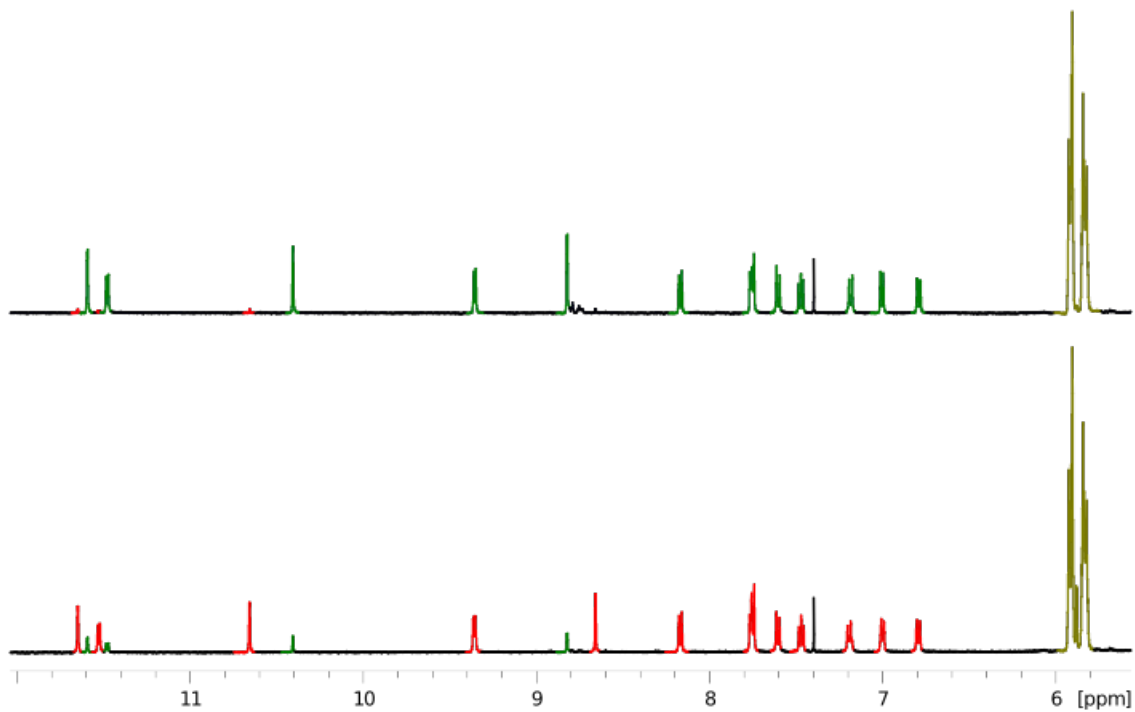
Binding constant (30 eq.) = $2.16 \times 10^3 \text{ L mol}^{-1}$

Binding constant (40 eq.) = $2.11 \times 10^3 \text{ L mol}^{-1}$

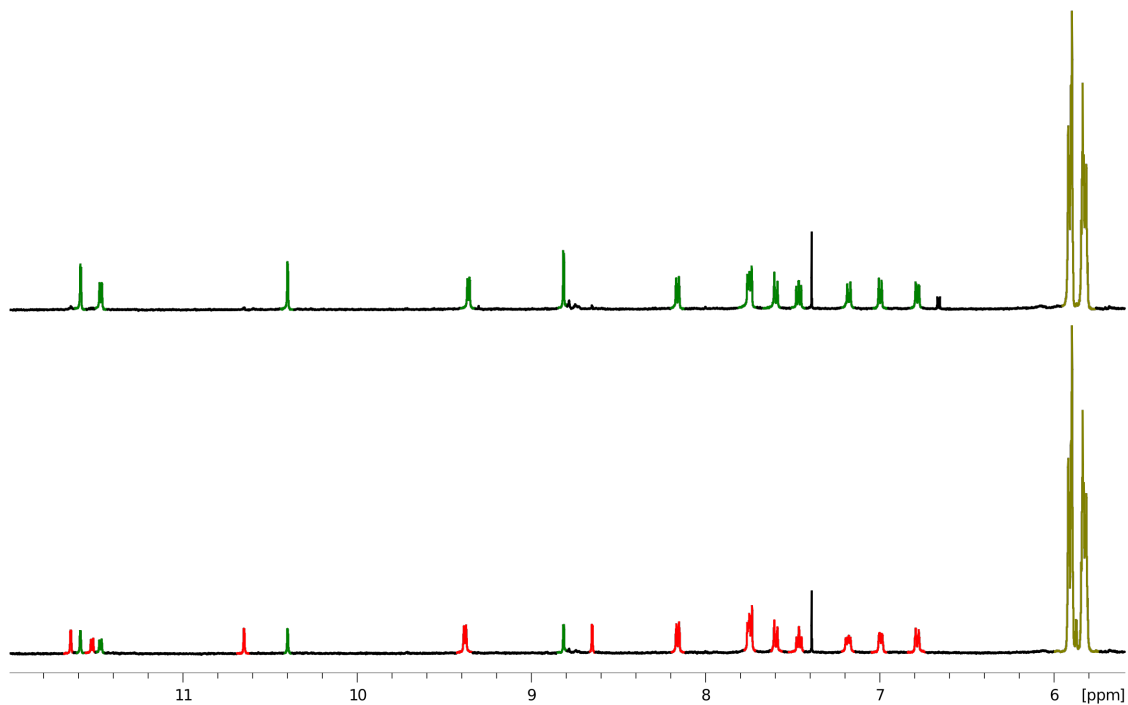
The given binding constant is the average value of all three = $2.15 \times 10^3 \text{ L mol}^{-1}$.



[2Cl@Pd₄L₈] after addition of 20 eq. 1,3-cyclohexadiene.
 Bottom: Immediately after addition. Top: after equilibration.



[2Cl@Pd₄L₈] after addition of 30 eq. 1,3-cyclohexadiene.
 Bottom: Immediately after addition. Top: after equilibration.



[2Cl@Pd₄L₈] after addition of 40 eq. 1,3-cyclohexadiene.
 Bottom: Immediately after addition. Top: after equilibration.

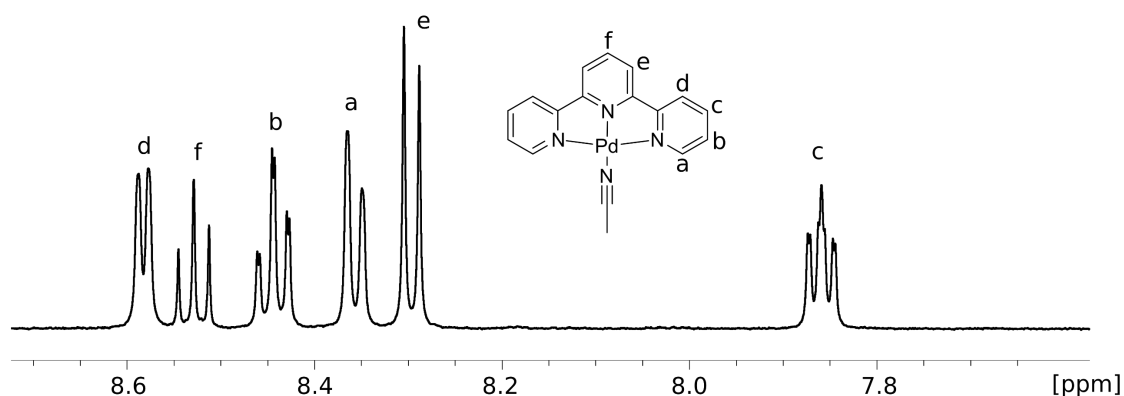
Preparation of [Pd₂L₄]

The acridone-based, monomeric cage was prepared according to previously published procedure.²

Preparation of [Pd(terpy)CH₃CN]

The complex was prepared by slight modification of a literature procedure.³ 2,2':6,2'-Terpyridine (20 mg, 85.47 μmol, 1 eq.) and [Pd(CH₃CN)₄(BF₄)₂] (38.9 mg, 85.47 μmol 1 eq.) were dissolved in 1.5 mL CH₃CN and the suspension was gently heated to 40 °C over night. The solid was filtered off and the solvent removed under reduced pressure. The crude was redissolved in CH₃CN and precipitated by addition of diethyl ether to obtain the pure product. Yield: 21 mg (63%).

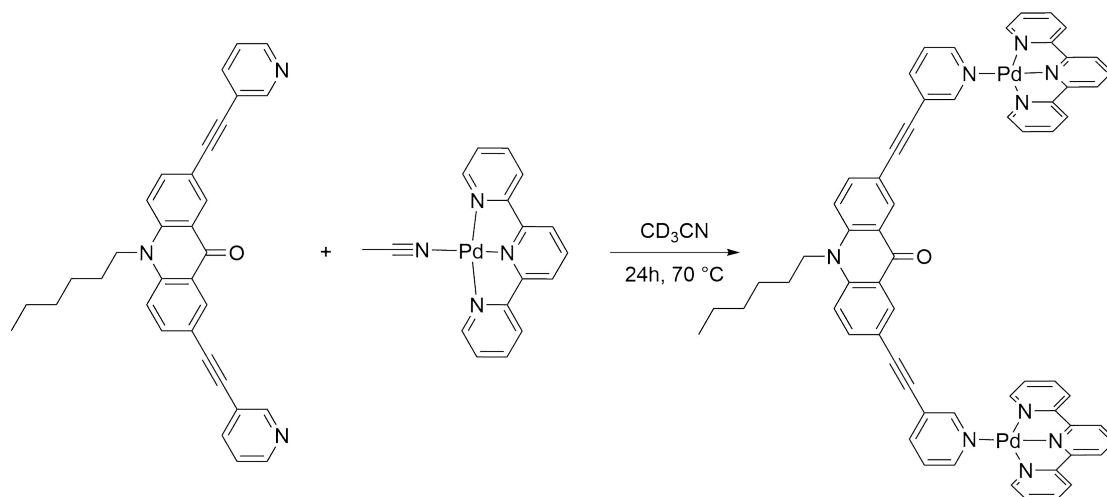
¹H-NMR (500 MHz, 298 K, CD₃CN): δ (ppm) = 8.59 (d, ³J = 5.10 Hz, 2H, d), 8.53 (t, ³J = 8.16 Hz, 1H, f), 8.45 (m, 2H, b), 8.36 (d, ³J = 7.90 Hz, 2H, a), 8.30 (d, ³J = 8.16 Hz, 2H, e), 7.86 (m, 2H, c).

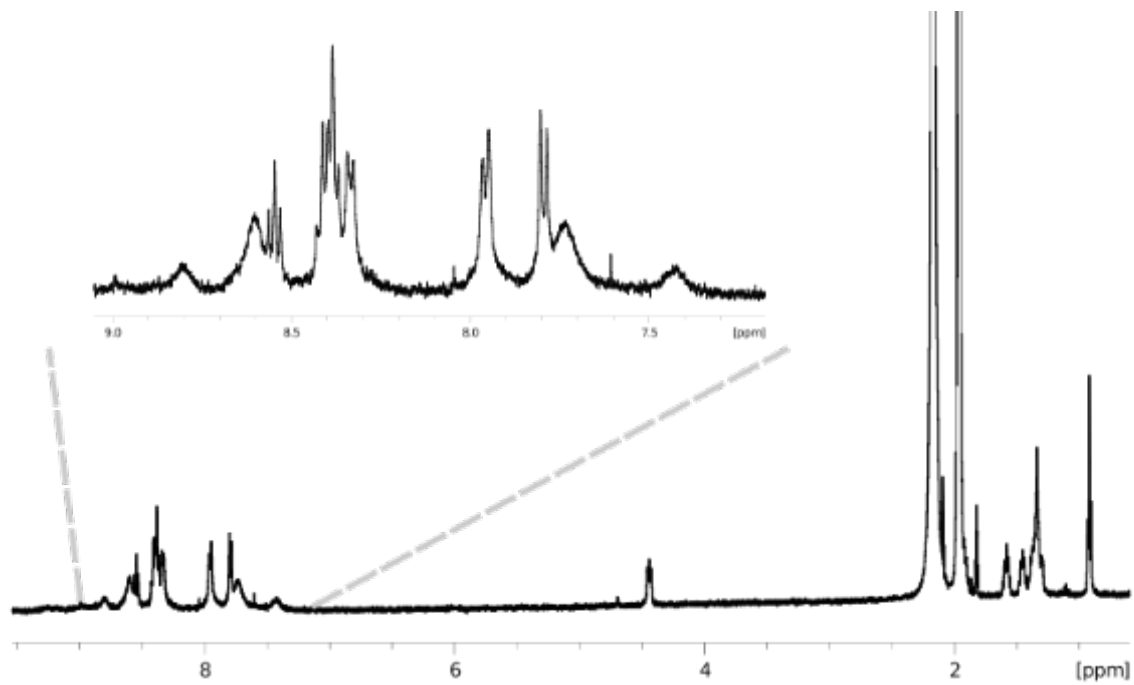


Preparation of [L(Pd-terpy)₂]

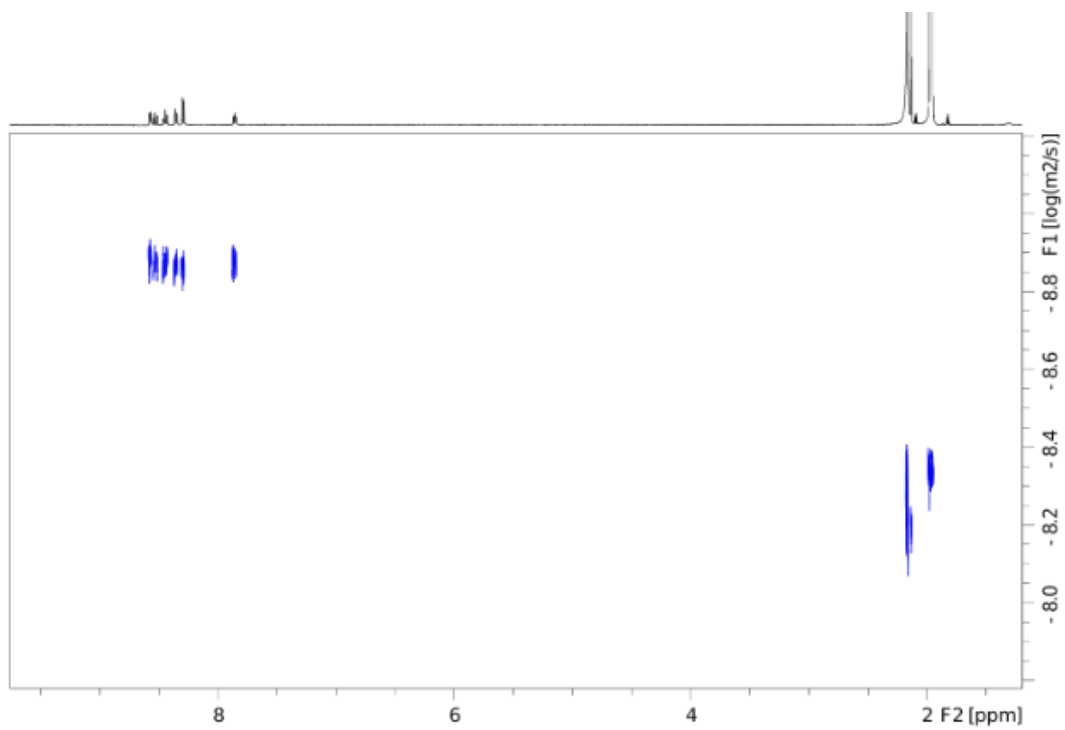
To a solution of acridone ligand L (60 μ L 7 mM in CD₃CN) was added a solution of [Pd(terpy)CH₃CN] (60 μ L, 15 mM in CD₃CN) and 480 μ L CD₃CN. The mixture was heated to 70 °C for 24h. Complete transformation of the complex was observed by ¹H-NMR spectroscopy. The ¹H-NMR spectrum of [L(Pd-terpy)₂] suffers from partial signal broadening, which we denote to rotational dynamics of the Pd-terpy units with respect to the bridging ligands. In order to further confirm successful formation of the complex, ¹H-DOSY spectra of [L(Pd-terpy)₂] and [Pd(terpy)CH₃CN] were compared. While [Pd(terpy)CH₃CN] shows a diffusion coefficient of 1.342×10^{-9} , corresponding to a hydrodynamic radius of 4.7 Å (at 298 K in acetonitrile), [L(Pd-terpy)₂] shows a lower diffusion coefficient (9.193×10^{-10}), corresponds to a hydrodynamic radius of 6.88 Å which is in agreement with the expected increase in size for the dinuclear complex.

The hydrodynamic radii were calculated from the measured diffusional coefficients (performing a T1 area fit of the corresponding signals) using the Stokes Einstein Equation. This is valid for spherical molecules. In our case, we assume a spherical shape for [L(Pd-terpy)₂] as well as for the double cage [Pd₄L₈], because the values are only compared qualitatively.

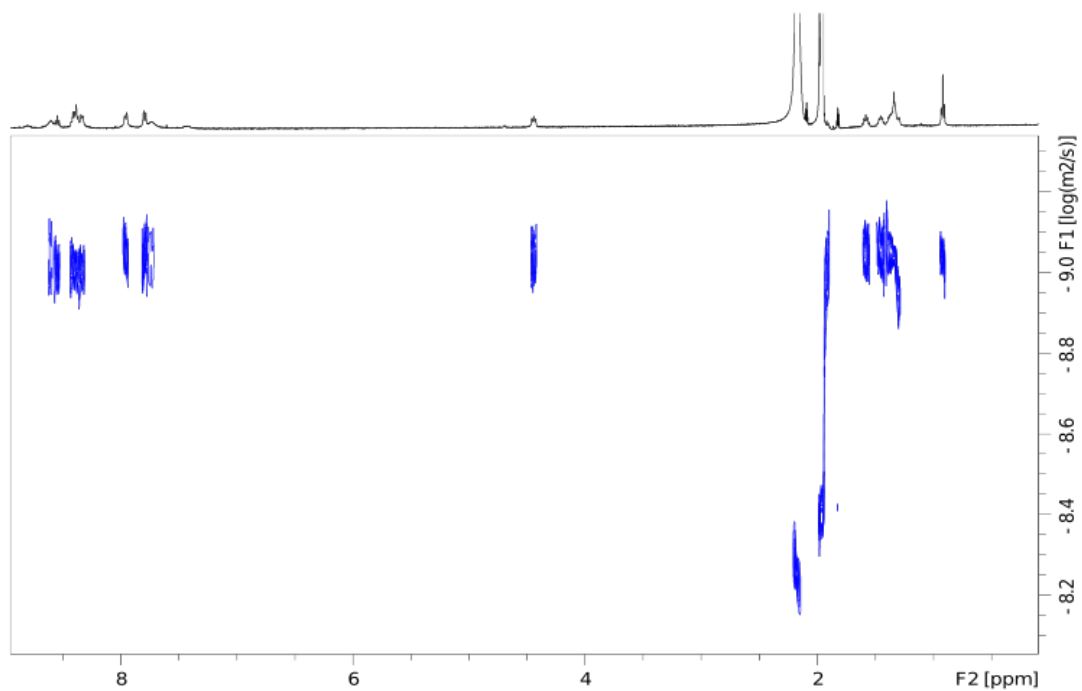




¹H NMR spectrum of [L(Pd-terpy)₂] (2.8 mM in CD₃CN, 298 K).



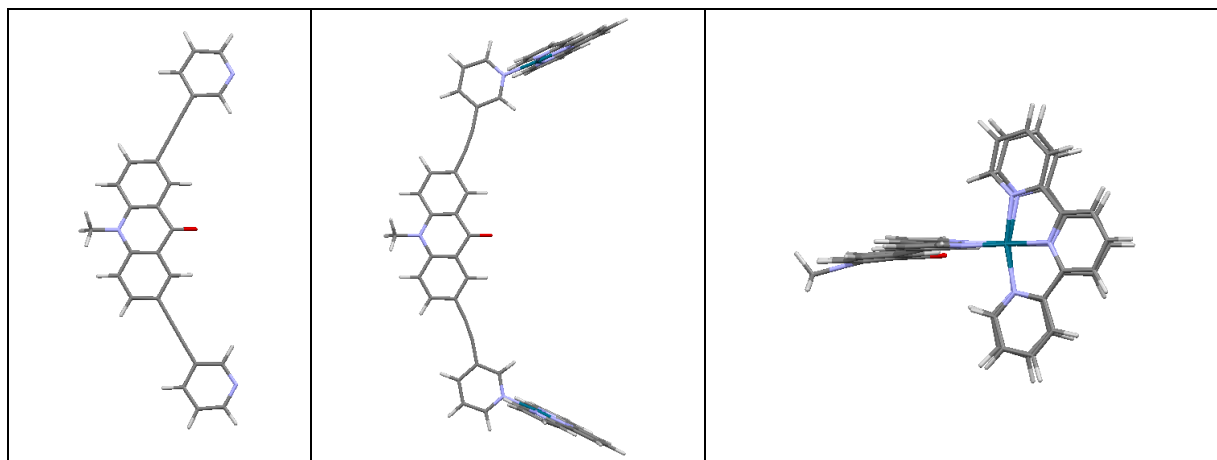
¹H DOSY spectrum of [Pd(terpy)CH₃CN] (1.4 mM in CD₃CN, 298 K).



^1H DOSY spectrum of $[\text{L}(\text{Pd-terpy})_2]$ (1.4 mM in CD_3CN , 298 K).

Models of $[\text{L}(\text{Pd-terpy})_2]$ and L

Structures were geometry optimized in ORCA⁴ using the B97-3c density functional approximation⁵ with general applicability for chemical properties of large systems.



Left: Model structure of L. Middle: side view of model structure of $[\text{L}(\text{Pd-terpy})_2]$ and right: Top view of $[\text{L}(\text{Pd-terpy})_2]$.

Further supporting figures and tables

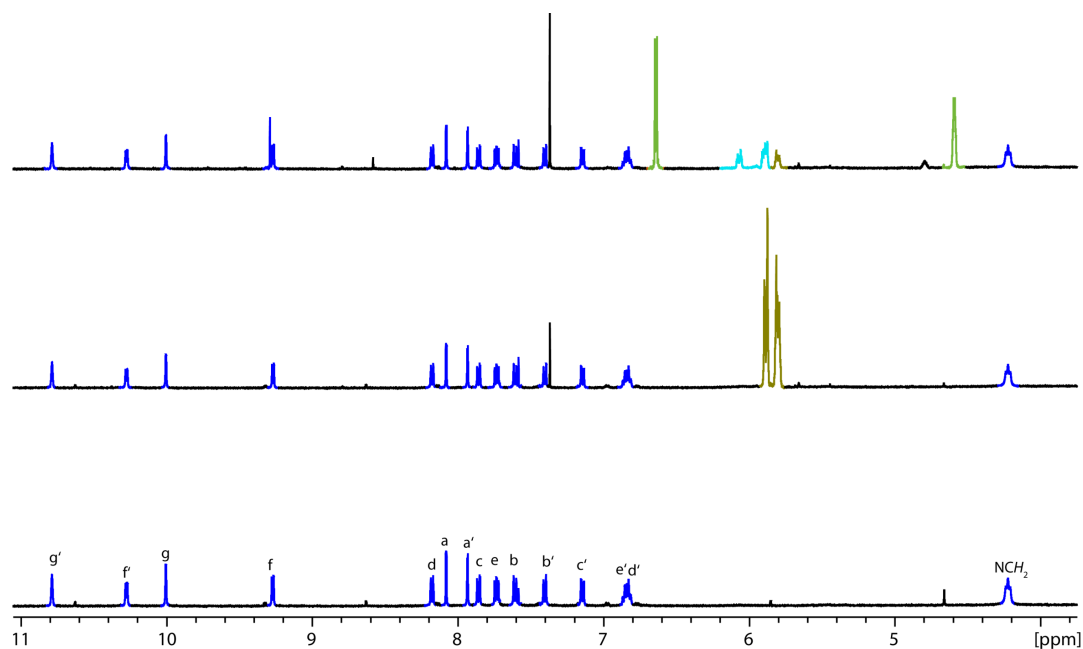


Figure S1. ^1H NMR (500 MHz, CD_3CN , 298 K) spectra (0.35 mM) of $[\mathbf{3BF}_4@\text{Pd}_4\text{L}_8]$ (blue) before (bottom) and after addition of **1** (gold) (30 eq.) (middle). Top: Mixture after irradiation for 40 minutes (365 nm LED) with product **2** (lime) and byproduct **3** (light blue).

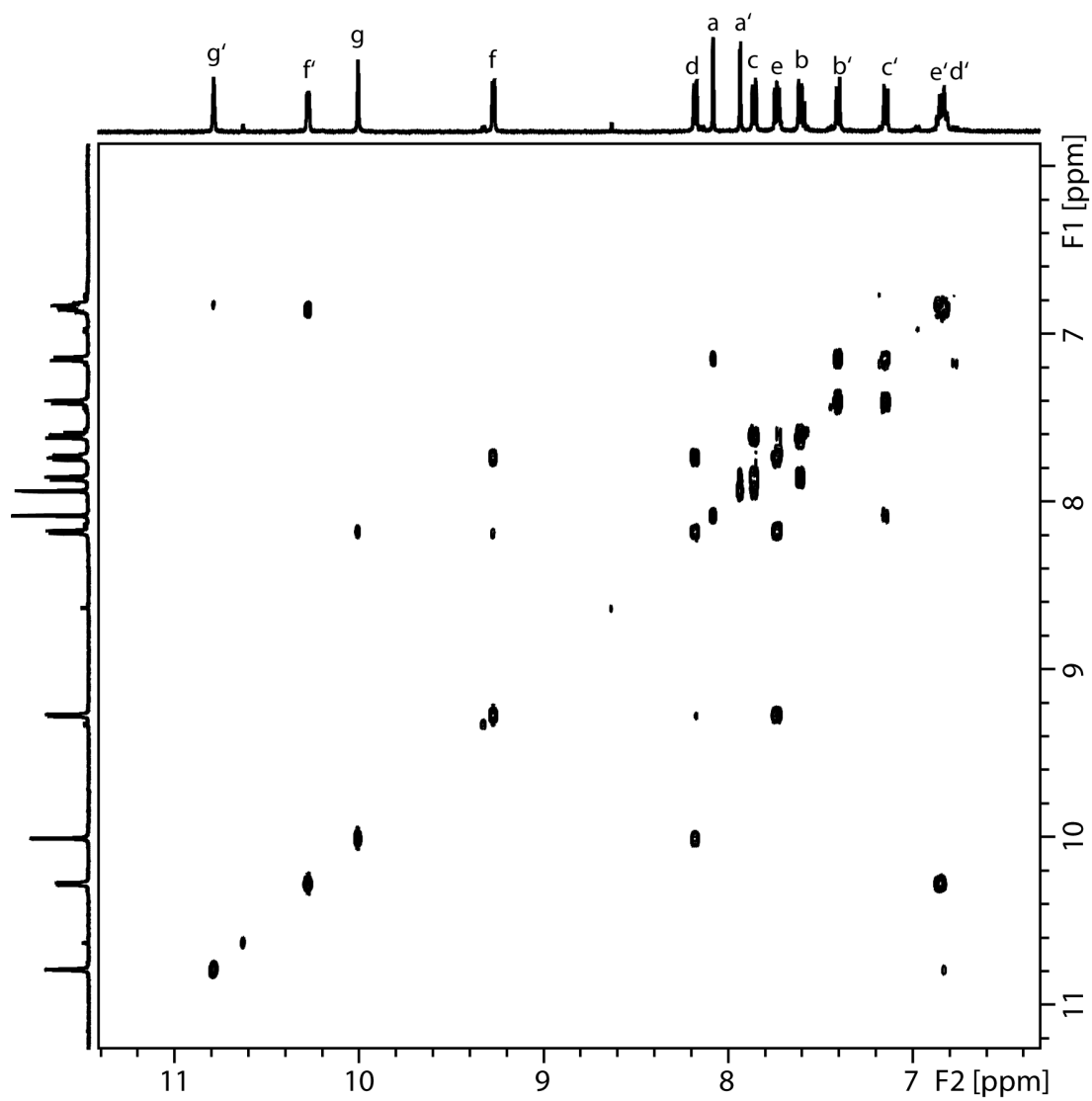


Figure S2. ^1H - ^1H COSY NMR (500 MHz, CD_3CN , 298 K) spectrum of $[\mathbf{3BF}_4@\text{Pd}_4\text{L}_8]$ (0.35 mM).

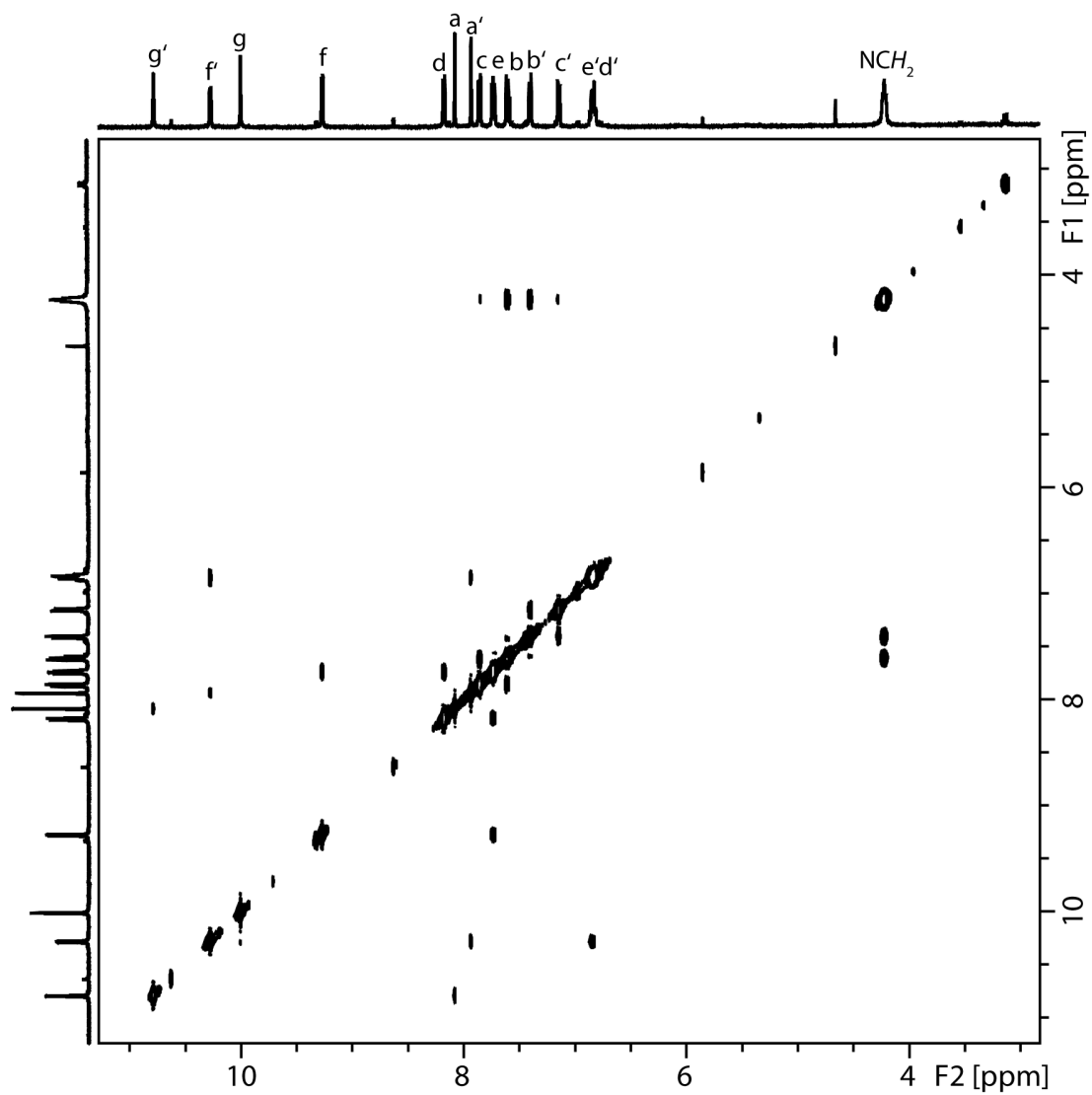


Figure S3. ^1H - ^1H NOESY NMR (500 MHz, CD_3CN , 298 K) spectrum of $[\text{3BF}_4@Pd_4L_8]$ (0.35 mM).

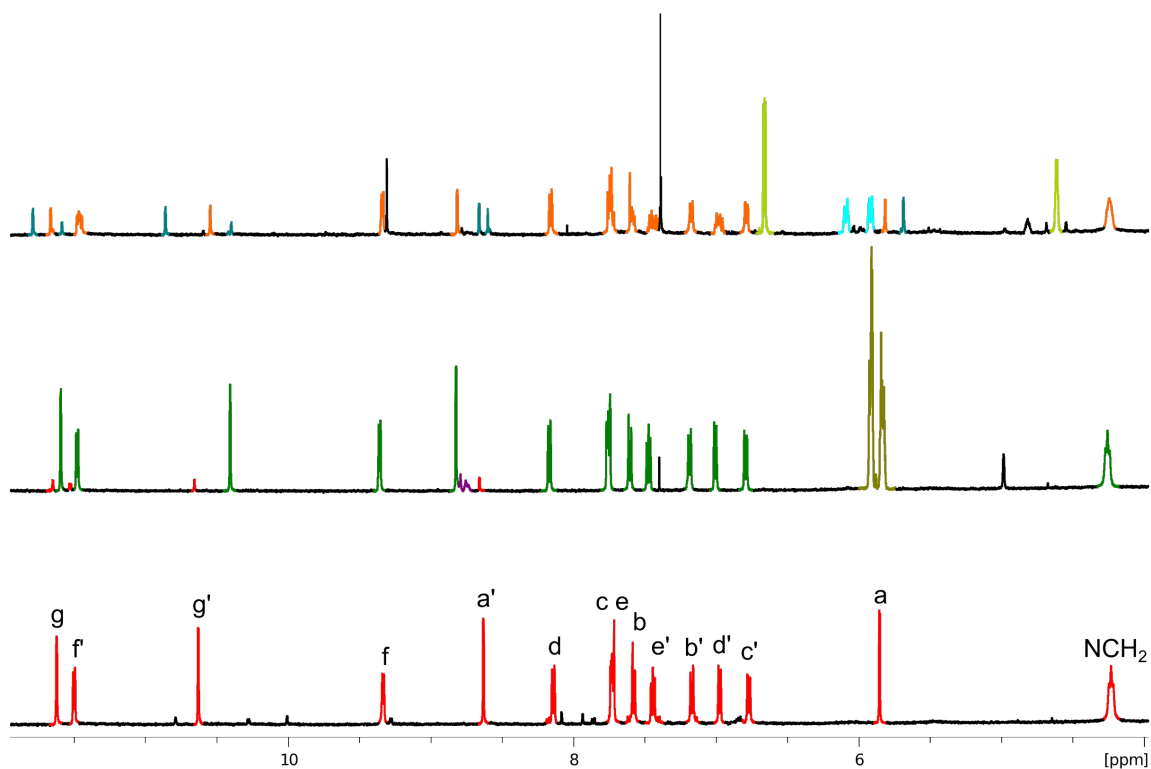


Figure S4. ^1H NMR (500 MHz, CD_3CN , 298 K) spectra in (0.35 mM) of $[\mathbf{2Cl@Pd}_4\mathbf{L}_8]$ (red) (bottom). Middle: 24h after addition of **1** (gold) (30 eq.); major species $[\mathbf{2Cl+C}_6\mathbf{H}_8\mathbf{@Pd}_4\mathbf{L}_8]$ (green). Top: Product mixture $[\mathbf{2Cl+C}_6\mathbf{H}_8\mathbf{O}_2\mathbf{@Pd}_4\mathbf{L}_8]$ (orange), **2** (lime) and **3** (light blue) after irradiation for 40 minutes with 365 nm LED. Cyan signals (top) result from splitting of the g, g' and a' signals, probably due to encapsulation of side product **3** in different orientation.

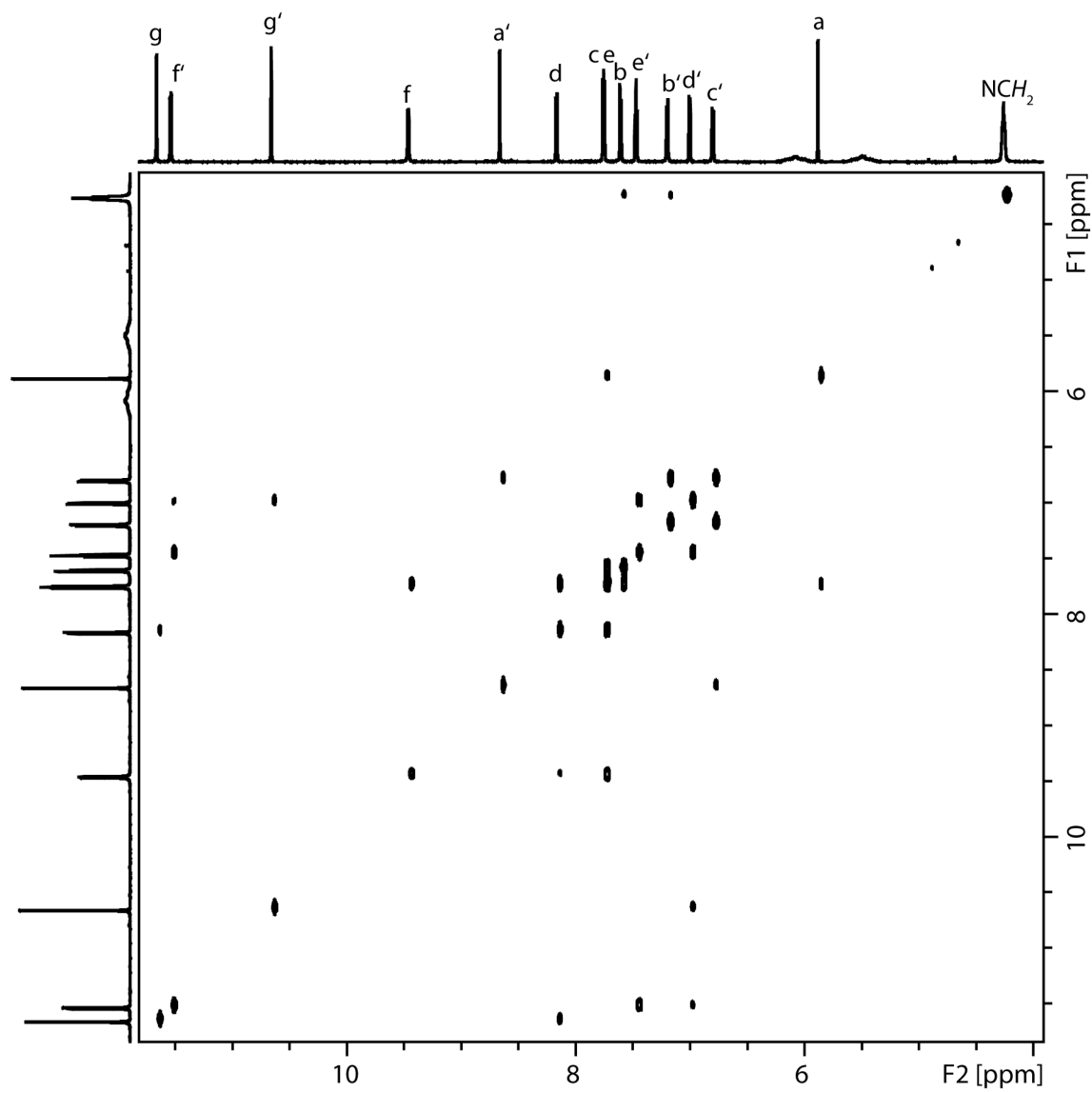


Figure S5. ^1H - ^1H COSY NMR (500 MHz, CD_3CN , 298 K) spectrum of $[2\text{Cl}@Pd_4L_8]$ (0.35 mM).

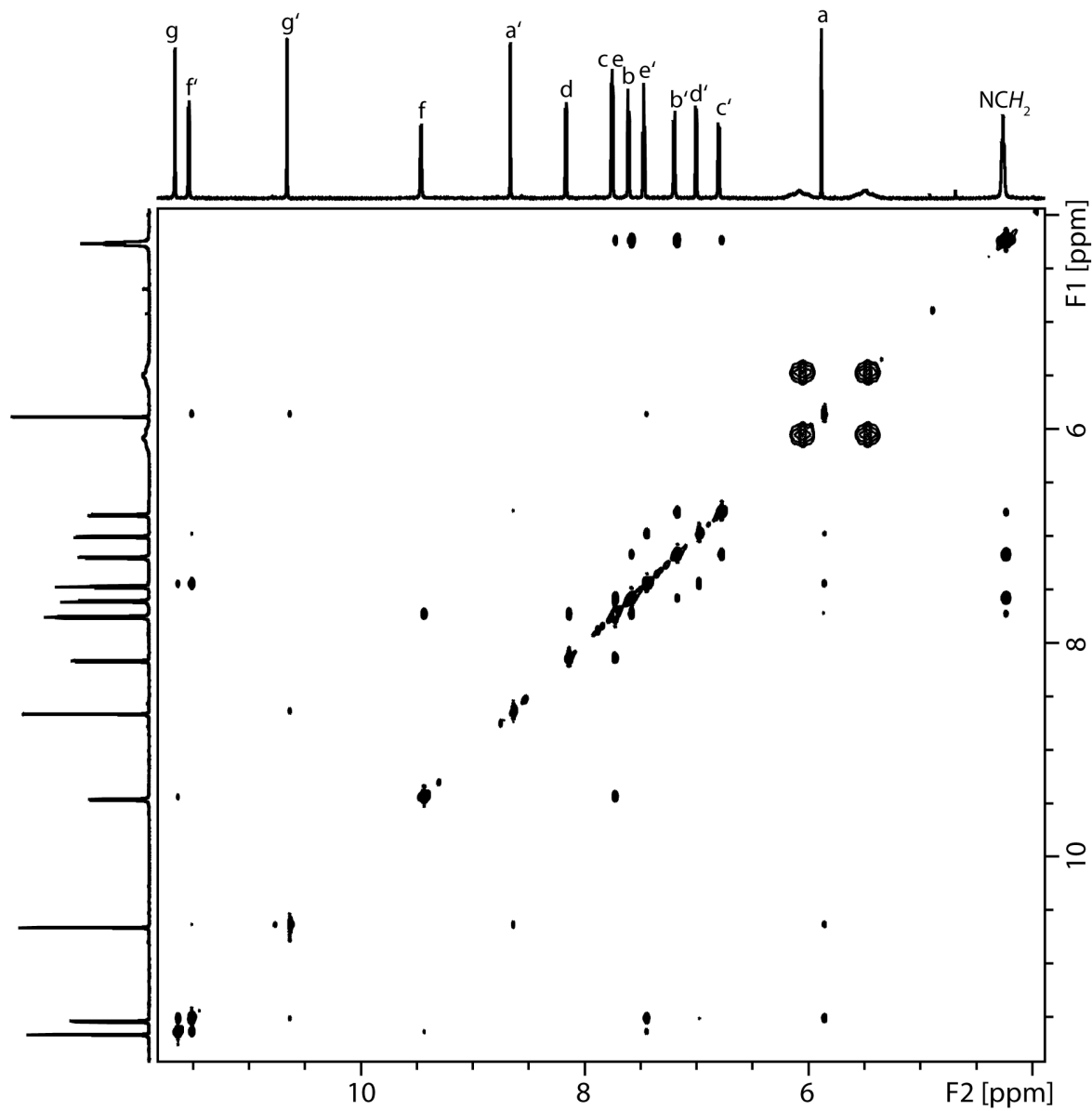


Figure S6. ^1H - ^1H NOESY NMR (500 MHz, CD_3CN , 298 K) spectrum of $[\mathbf{2Cl@Pd}_4\mathbf{L}_8]$ (0.35 mM).

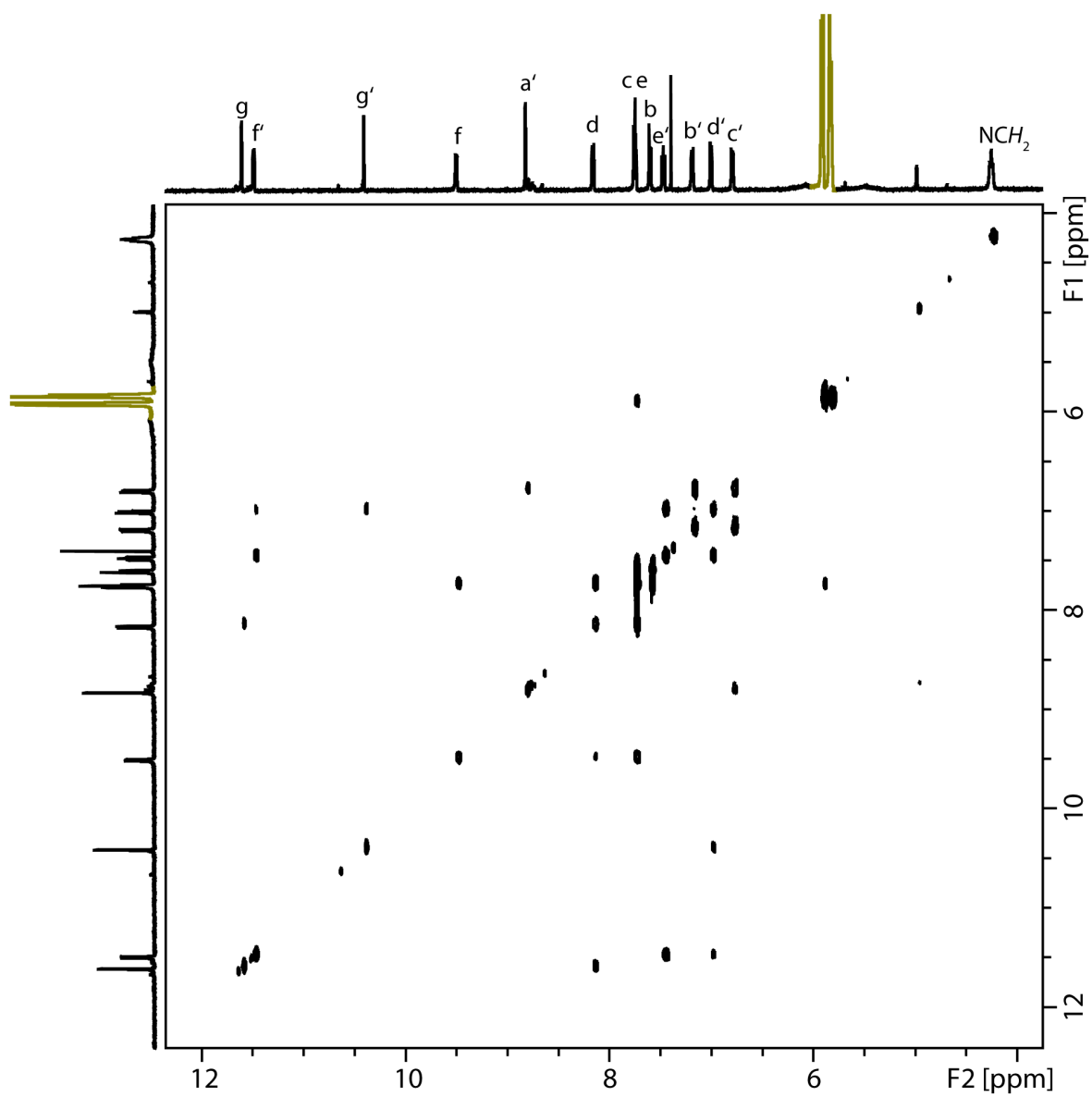


Figure S7. ^1H - ^1H COSY NMR (500 MHz, CD_3CN , 298 K) spectrum of $[\mathbf{2Cl}+\text{C}_6\text{H}_8@\text{Pd}_4\text{L}_8]$ (0.35 mM) in presence of 30 eq. **1** (gold).

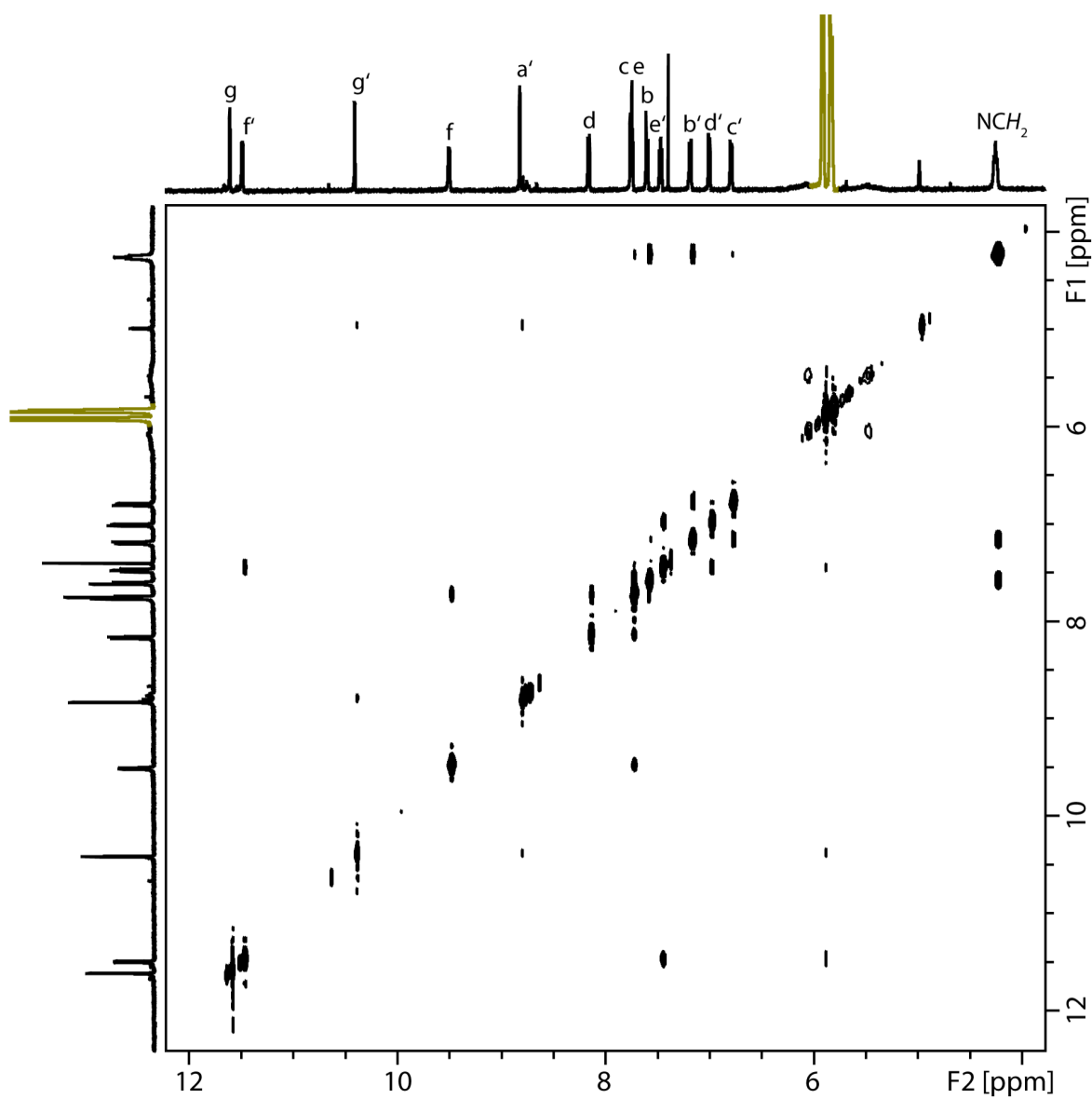


Figure S8. ^1H - ^1H NOESY NMR (500 MHz, CD_3CN , 298 K) spectrum of $[\mathbf{2Cl}+\text{C}_6\text{H}_8@\text{Pd}_4\text{L}_8]$ (0.35 mM) in presence of 30 eq. **1** (gold).

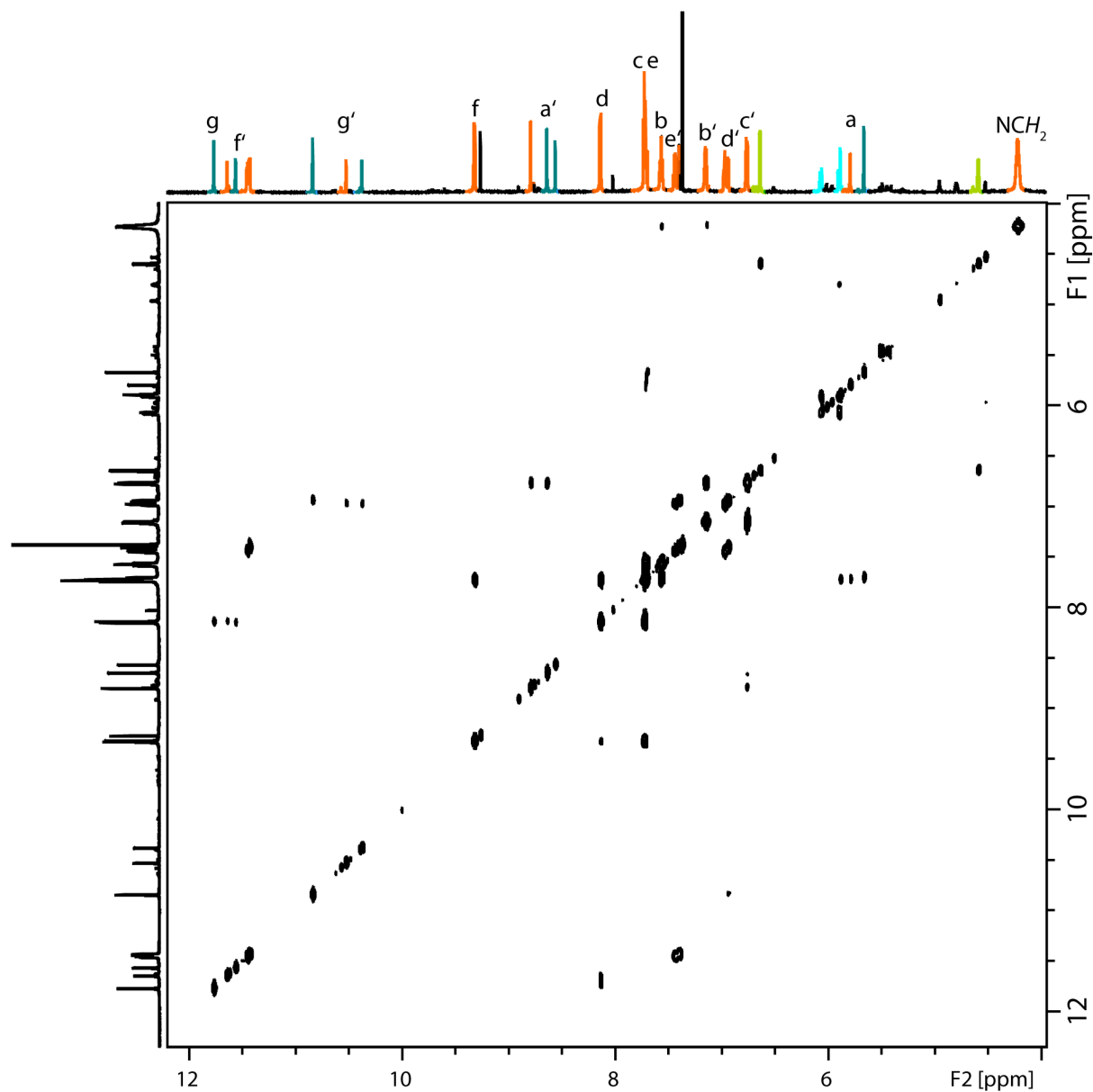


Figure S9: ¹H-¹H COSY NMR (700 MHz, CD₃CN, 298 K) spectrum of [2Cl@Pd₄L₈] (0.35 mM) after irradiation for 40 minutes (365 nm LED). Orange signals are major product [2Cl+C₆H₈O₂@Pd₄L₈]. Green signals correspond to free product **2**. Blue signals arise from encapsulated side product **3**.

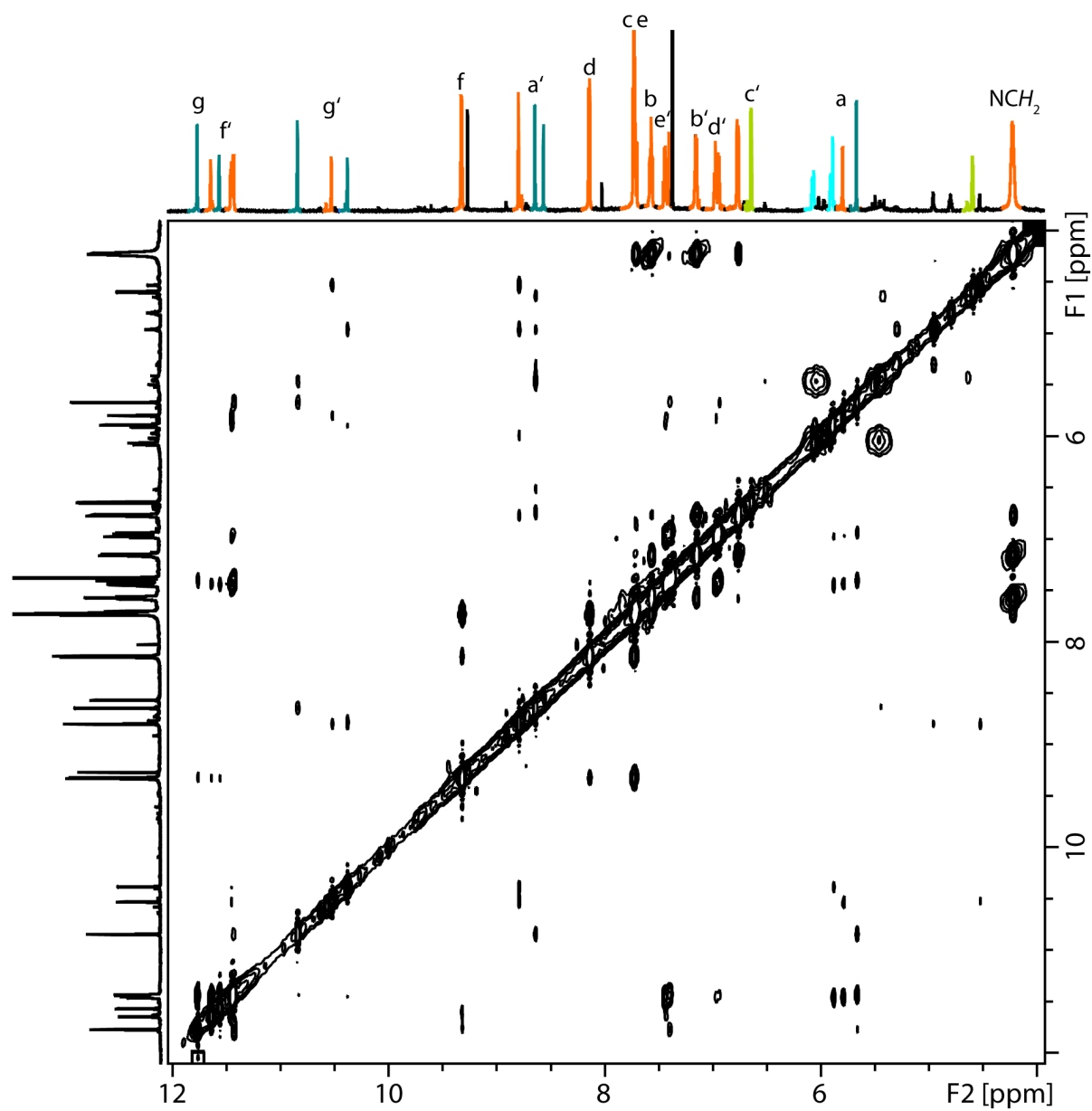


Figure S10: ¹H-¹H NOESY NMR (700 MHz, CD₃CN, 298 K) spectrum of [2Cl@Pd₄L₈] (0.35 mM) after irradiation for 40 minutes (365 nm LED). Orange signals are major product [C₆H₈O₂@Pd₄L₈]. Green signals correspond to free product **2**. Blue signals arise from encapsulated side product **3**.

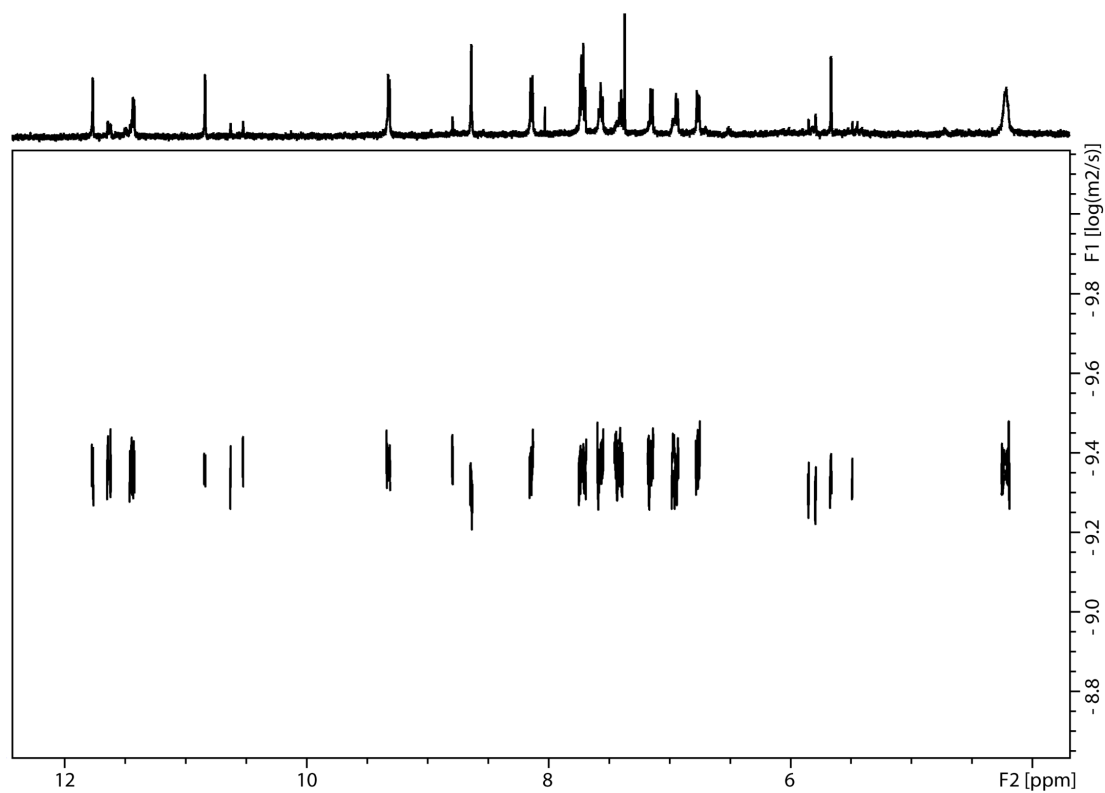


Figure S11: ^1H DOSY NMR (500 MHz, CD_3CN , 298 K) of final product $[\mathbf{2Cl}+\text{C}_6\text{H}_8\text{O}_2@\text{Pd}_4\text{L}_8]$ after irradiation.

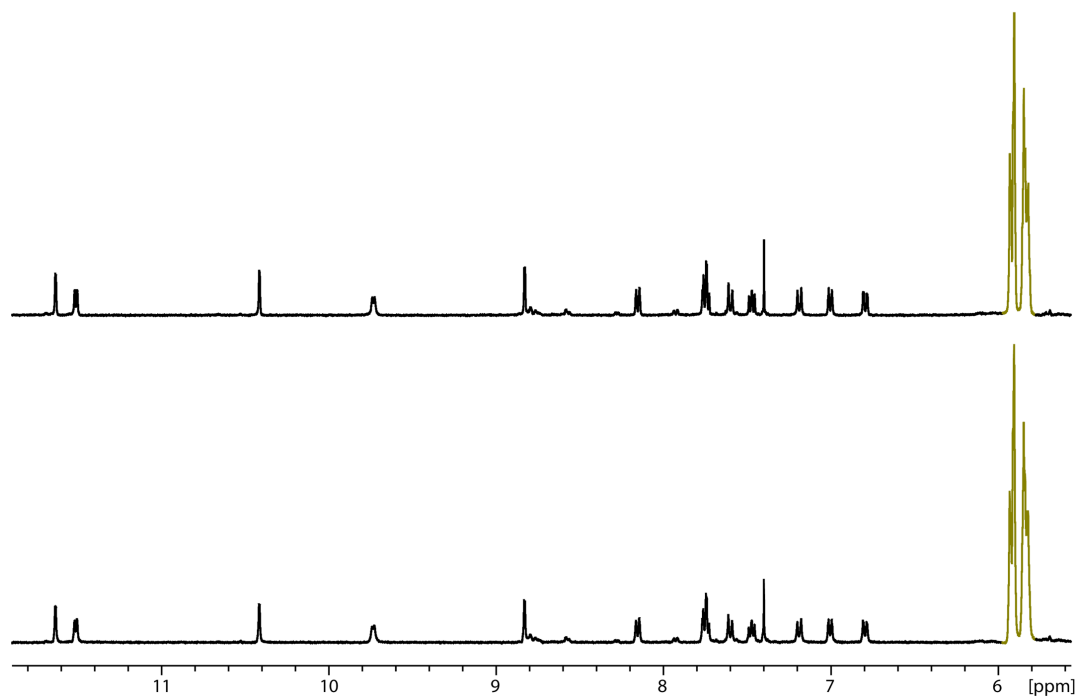


Figure S12: ^1H NMR (500 MHz, CD_3CN , 298 K) of $[\mathbf{2Cl}+\text{C}_6\text{H}_8@\text{Pd}_4\text{L}_8]$ (0.35 mM) in presence of 10 eq. **1** after 34 d under Ar atmosphere (bottom) and after 43 d under Ar atmosphere (top) in presence of light. No transformation of **1** into **2** or **3** is observed.

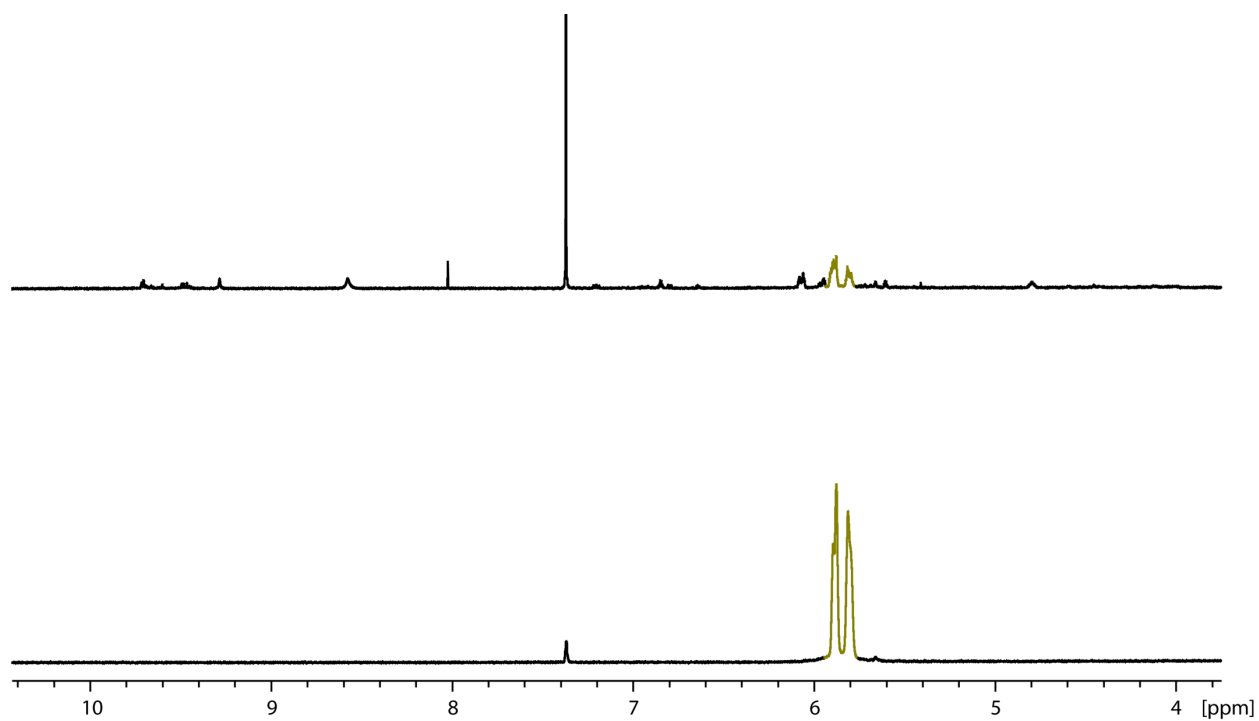


Figure S13. ^1H NMR (500 MHz, CD_3CN , 298 K) spectra of **1** (gold, 70 mM) before (bottom) and after (top) irradiation for 40 minutes with 365 nm LED.

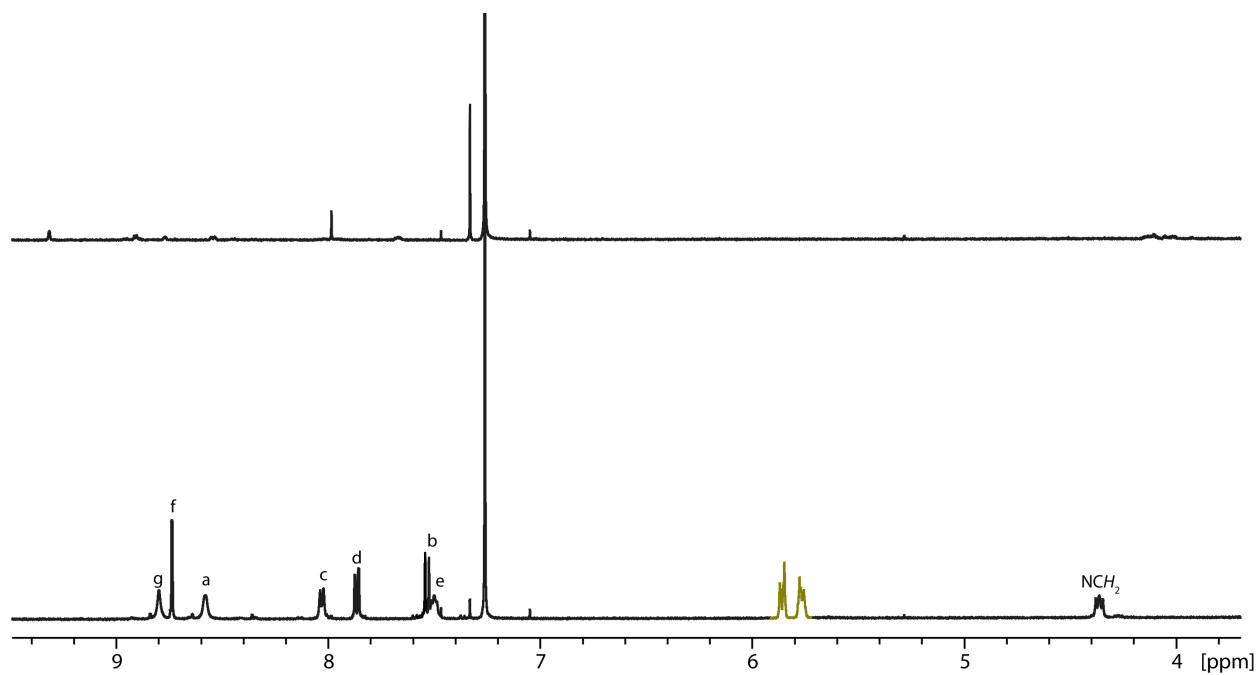


Figure S14. ^1H NMR (500 MHz, CDCl_3 , 298 K) spectra of acridone ligand (2.8 mM) in presence of **1** (gold) before (bottom) and after (top) irradiation.

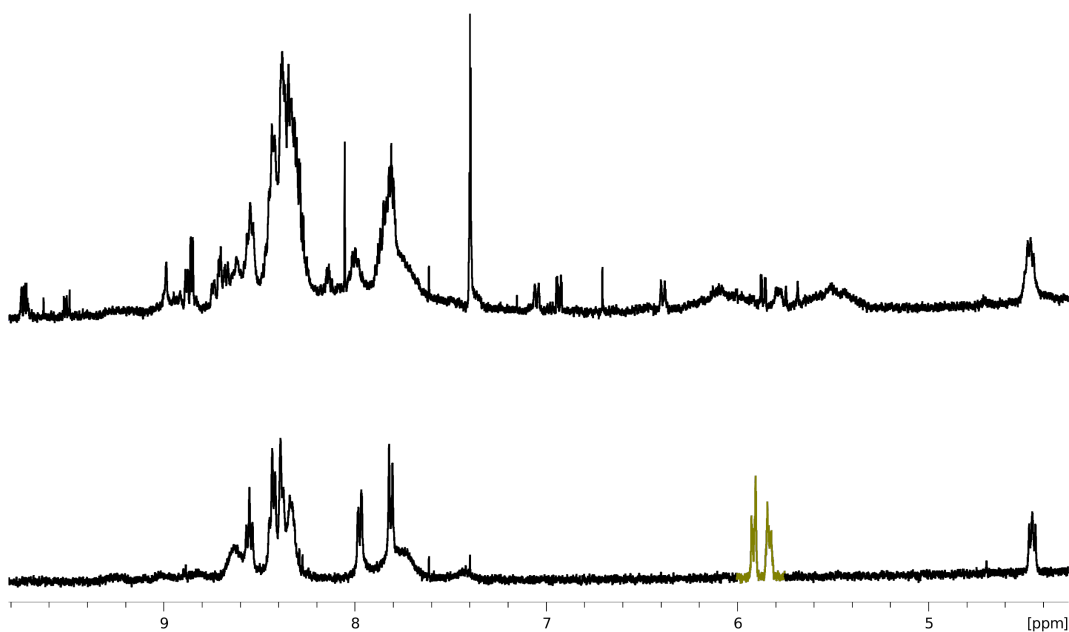


Figure S15. ^1H NMR (500 MHz, CD_3CN , 298 K) spectra of $[(\text{L})\text{Pd}(\text{terpy})]$ (bottom) with 30 eq. **1** (gold) and after irradiation for 40 minutes with 365 nm LED (top). No formation of product **2** or side product **3** are observed.

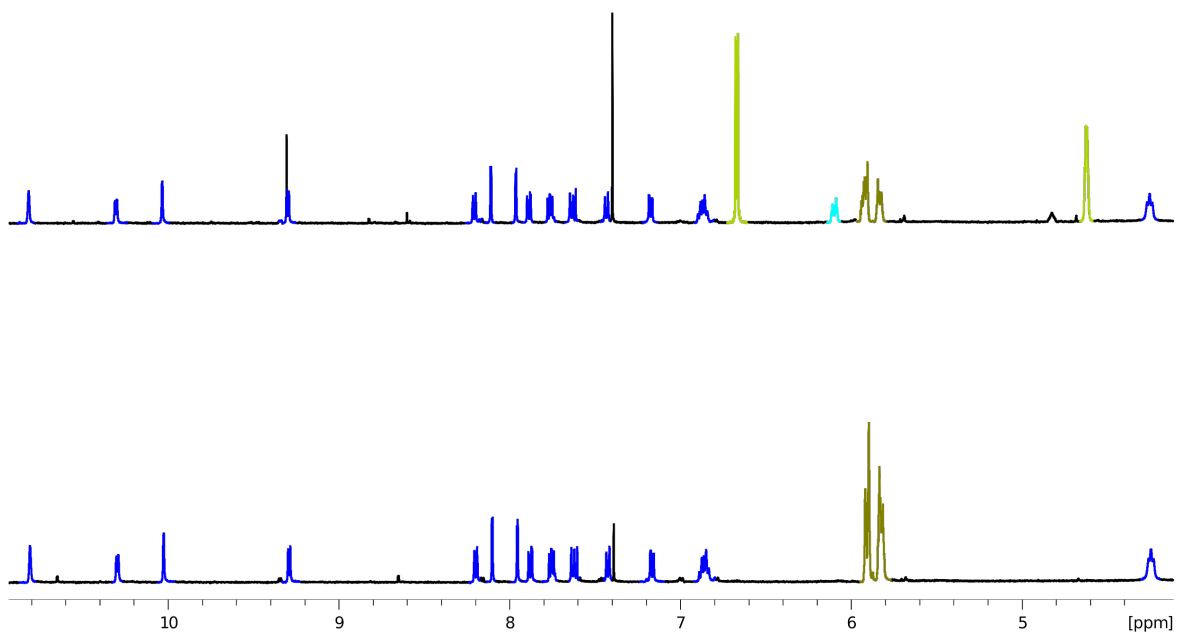


Figure S16. ^1H NMR (500 MHz, CD_3CN , 298 K) spectra of $[\text{BF}_4@\text{Pd}_4\text{L}_3]$ (blue) (bottom) with 30 eq. **1** (gold) and after irradiation for 40 minutes with 365 nm LED with intensity reduced to 50% (top). Both product **2** (lime) and side product **3** (light blue) are observed.

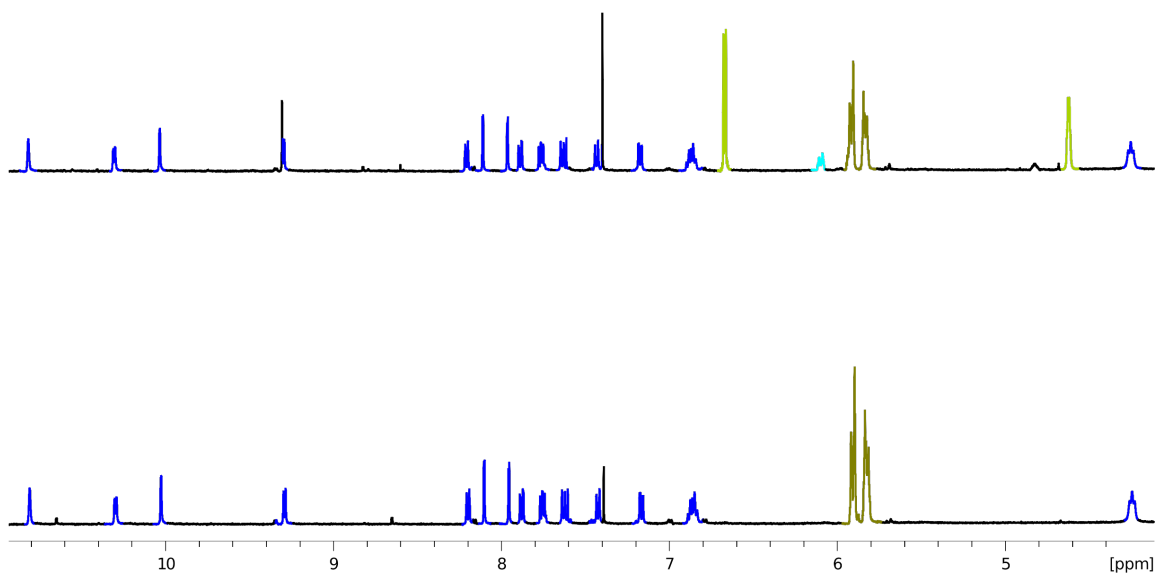


Figure S17. ^1H NMR (500 MHz, CD_3CN , 298 K) spectra of $[\text{BF}_4@Pd_4L_3]$ (blue) (bottom) with 30 eq. **1** (gold) and after irradiation for 40 minutes with 365 nm LED with intensity reduced to 20% (top). Both product **2** (lime) and side product **3** (light blue) are observed.

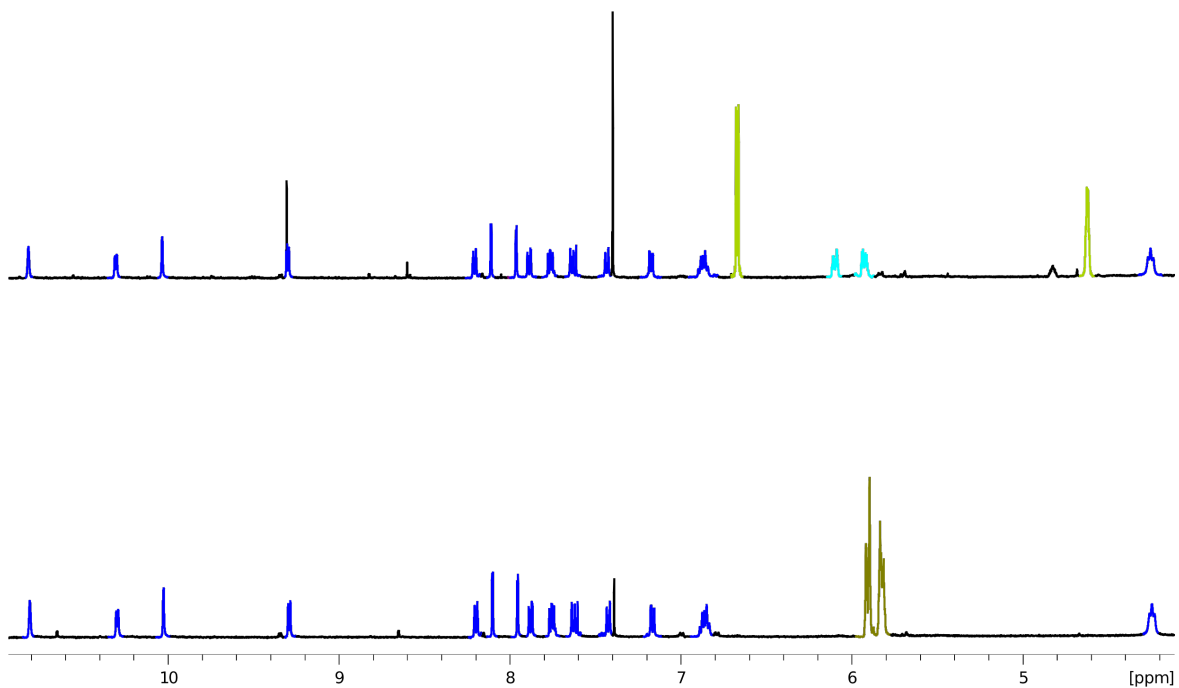


Figure S18 ^1H NMR (500 MHz, CD_3CN , 298 K) spectra of $[\text{BF}_4@Pd_4L_3]$ (blue) (bottom) with 30 eq. **1** (gold) and after irradiation for 40 minutes with 365 nm LED at 5 °C (top). Both product **2** (lime) and side product **3** (light blue) are observed.

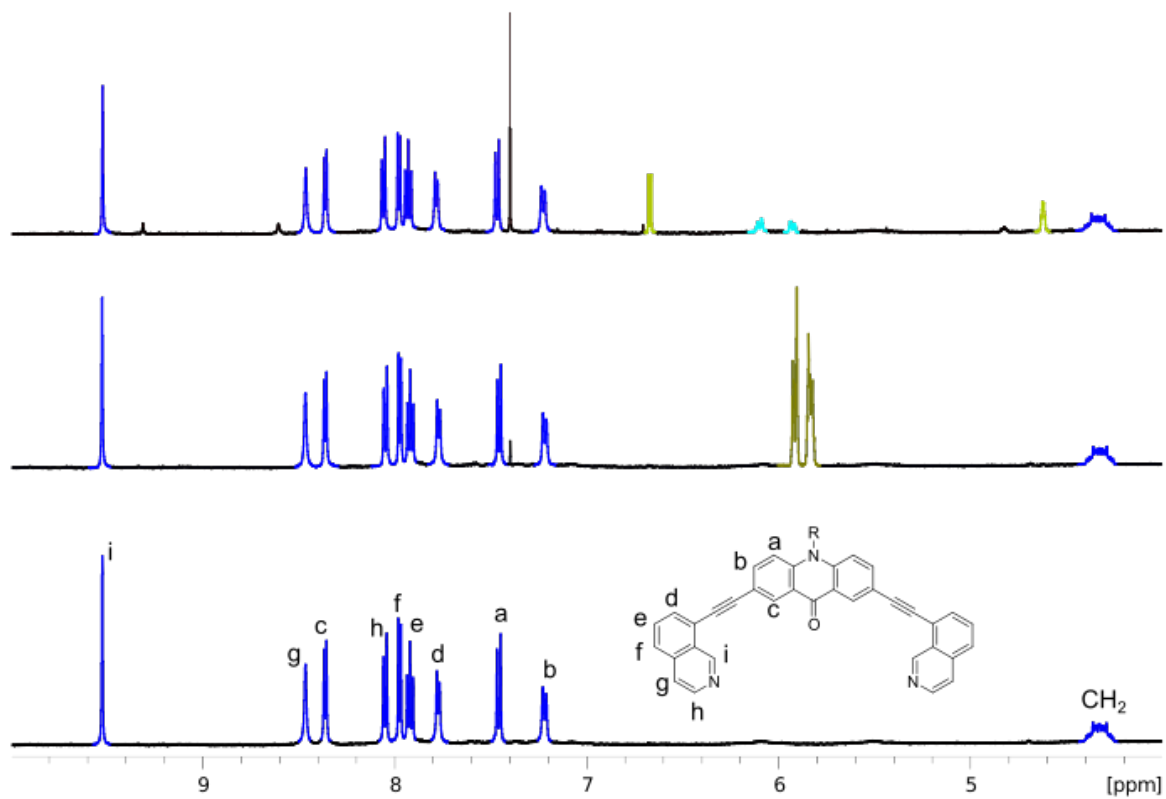


Figure S19 ^1H NMR (500 MHz, CD_3CN , 298 K) spectra of $[\text{Pd}_2\text{L}_4]$ (blue) (bottom), after addition of 30 eq. **1** (gold, middle) and after irradiation for 40 minutes with 365 nm LED (top). Both product **2** (lime) and side product **3** (light blue) are observed.

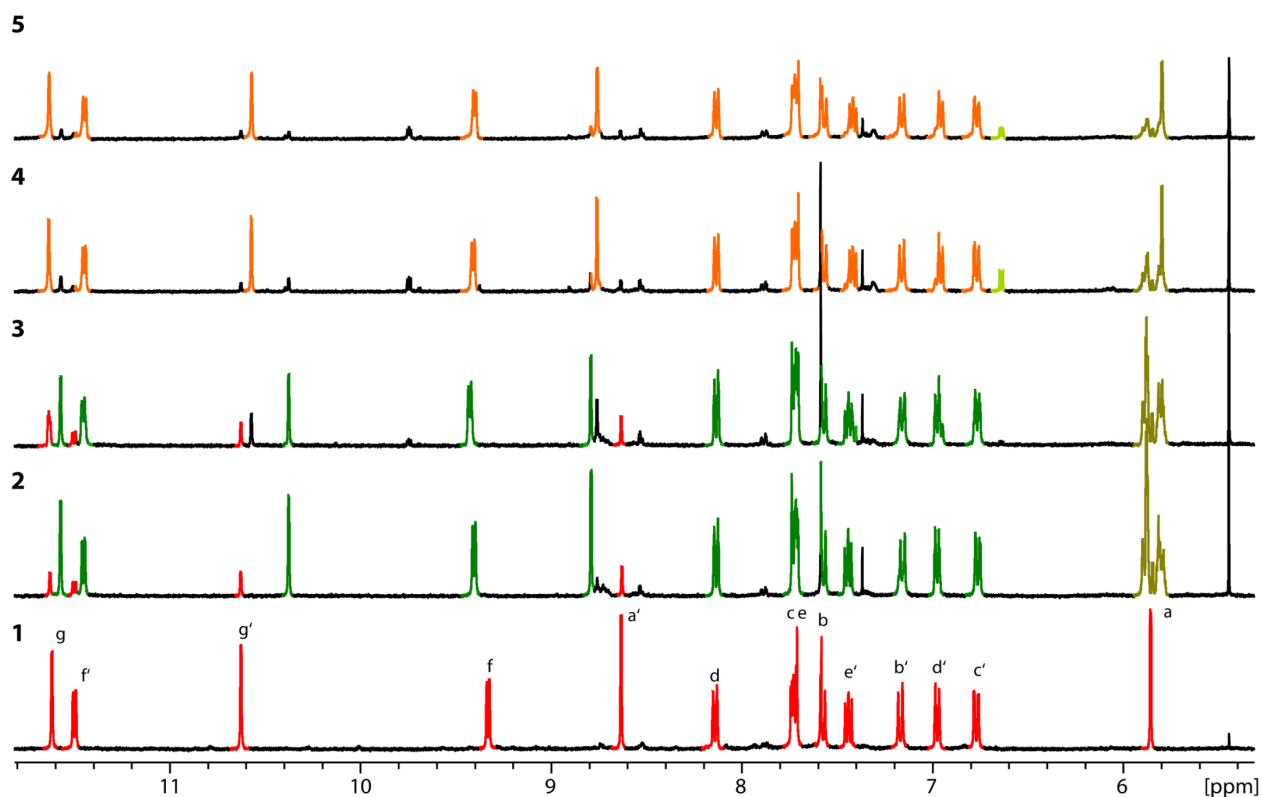


Figure S20: ^1H NMR (500 MHz, CD_3CN , 298 K) of $[\mathbf{2Cl@Pd}_4\text{L}_8]$ (0.35 mM) in presence of oxygen (red, 1), 1 d after addition of **1** at rt (green, 2) and 22 d after addition of **1** at rt (3). After 50 d (4), the cage signals start to change (orange), signals of **1** are reduced (gold) and a new species arises (lime) which represents the free product **2**. Final cage spectrum after 94 d (orange, 5).

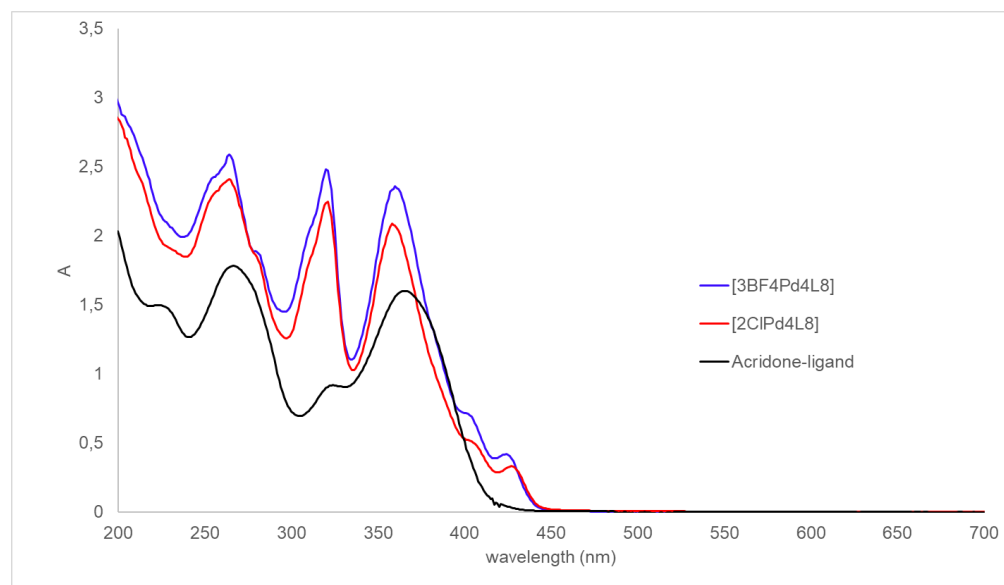


Figure S21. UV vis spectra of ligand (2.8 mM in CH_3CN) and cages (0.35 mM in CH_3CN) with pathlength 1 mm.

Crystallographic Details

Table 1. Crystal data and structure refinement for [2Cl+C₆H₈@Pd₄L₈] and [2Cl+C₆H₈O₂@Pd₄L₈]

Compound	[2Cl+C₆H₈@Pd₄L₈]	2Cl+C₆H₈O₂@Pd₄L₈
Compound Code	sl422	sl433
CCDC number	1952467	1952468
Empirical formula	C ₂₇₂ H ₂₂₇ B ₃ Cl ₂ F ₁₂ N ₂₅ O ₈ Pd ₄	C ₂₇₀ H ₂₂₄ B ₃ Cl _{2.50} F ₁₂ N ₂₄ O ₁₀ Pd ₄
Formula weight	4730.70	4739.37
Temperature [K]	80(2)	100(2)
Crystal system	tetragonal	tetragonal
Space group (number)	<i>P4/ncc</i> (130)	<i>P4/ncc</i> (130)
<i>a</i> [Å]	21.757(3)	21.837(2)
<i>b</i> [Å]	21.757(3)	21.837(2)
<i>c</i> [Å]	62.923(13)	62.930(6)
α [Å]	90	90
β [Å]	90	90
γ [Å]	90	90
Volume [Å ³]	29786(10)	30009(6)
<i>Z</i>	4	4
ρ_{calc} [g/cm ³]	1.055	1.049
μ [mm ⁻¹]	0.172	2.587
<i>F</i> (000)	9756	9766
Crystal size [mm ³]	0.100×0.100×0.020	0.100×0.100×0.050
Crystal colour	colourless	colourless
Crystal shape	plate	plate
Radiation	synchrotron ($\lambda=0.5636$)	CuK α ($\lambda=1.54178$)
2 θ range [°]	1.03 to 39.69	5.72 to 117.84
Index ranges	-26 ≤ <i>h</i> ≤ 26 -26 ≤ <i>k</i> ≤ 26 -75 ≤ <i>l</i> ≤ 75	-19 ≤ <i>h</i> ≤ 24 -23 ≤ <i>k</i> ≤ 18 -69 ≤ <i>l</i> ≤ 69
Reflections collected	335970	130428
Independent reflections	13615 <i>R</i> _{int} = 0.0515 <i>R</i> _{sigma} = 0.0145	10657 <i>R</i> _{int} = 0.1137 <i>R</i> _{sigma} = 0.0530
Completeness to $\theta = 19.765^\circ$	99.60	98.70
Data / Restraints / Parameters	13615/1640/820	10657/1658/841
Goodness-of-fit on <i>F</i> ²	2.566	2.135
Final <i>R</i> indexes [<i>I</i> ≥ 2 σ (<i>I</i>)]	<i>R</i> ₁ = 0.1608 <i>wR</i> ₂ = 0.5570	<i>R</i> ₁ = 0.1677 <i>wR</i> ₂ = 0.5024
Final <i>R</i> indexes [all data]	<i>R</i> ₁ = 0.1824 <i>wR</i> ₂ = 0.5754	<i>R</i> ₁ = 0.2156 <i>wR</i> ₂ = 0.5366
Largest peak/hole [eÅ ⁻³]	1.65/-0.93	4.33/-1.23

Measurement and processing details of [2Cl+C₆H₈@Pd₄L₈]

Crystals were obtained by slow vapor diffusion of ethyl ether into a solution of [2Cl+C₆H₈@Pd₄L₈] in Acetonitrile.

Suitable single crystals for X-ray structural analysis of were mounted at room temperature in NVH oil. Crystals were stored at cryogenic temperature in dry shippers, in which they were safely transported to macromolecular beamline P11⁶ at the Petra III synchrotron, DESY, Germany. X-ray diffraction data was collected at 80(2) K on a single axis goniometer, equipped with an Oxford Cryostream 800 low temperature device and a Pilatus 6M fast detector. The data integration and reduction were taken with XDS.⁷

Measurement and processing details of [2Cl+C₆H₈O₂@Pd₄L₈]

Crystals were obtained by slow vapor diffusion of ethyl ether into a solution of [2Cl+C₆H₈O₂@Pd₄L₈] in Acetonitrile.

Suitable single crystals of [c-C] were mounted in NVH oil on a nylon loop. X-ray diffraction data were collected on Bruker d8 venture systems based on a kappa goniometer with Incoatec microfocus X-ray sources (I μ S 2.0), Incoatec QUAZAR mirror optics and a Photon II detector. The data were collected at 100 K crystal temperature (Oxford Cryosystems CRYOSTREAM 800), 50 kV and 600 μ A and an appropriate 0.5° omega scan strategy. Data reduction was performed with SAINT v8.30C (Bruker, 2009a) out of the APEX II v2.2012.2 0 (Bruker, 2009b) program package. SADABS[S9] (version 2014/4) was employed for the incident beam scaling, determination of the spherical harmonic coefficients, outlier rejection and determination of the error model parameters.

Specific refinement details of [2Cl+C₆H₈@Pd₄L₈] and [2Cl+C₆H₈O₂@Pd₄L₈]

Both structures were solved by direct methods with SHELXT.⁸ They were refined by full-matrix least-squares against F² using SHELXL2014⁹ with the help of the SHELXle¹⁰ graphical user interface. The SQUEEZE¹¹ method provided by the program Platon¹² was used to improve the contrast of the electron density map the structure.

Stereochemical restraints for the Acridone ligands (ACR), educt (CHD), oxygen adduct guest (DOX) and BF₄ (BF₄) counter ions of both structures were generated by the GRADE program using the GRADE Web Server (<http://grade.globalphasing.org>) and applied in the refinement. A GRADE dictionary for SHELXL contains target values and standard deviations for 1,2-distances (DFIX) and 1,3-distances (DANG), as well as restraints for planar groups (FLAT). Due to the location of the THF on a special position (2-fold axis) the GRADE restraint dictionary was modified manually to cover symmetry generated atoms. All displacements for non-hydrogen atoms were refined anisotropically. The refinement of ADP's for carbon, nitrogen and oxygen atoms was enabled by a combination of similarity restraints (SIMU) and rigid bond restraints (RIGU).¹³

Overlap of both guest positions with the crystallographic fourfold axis makes the unequivocal interpretation of the exact guest molecule's chemistry impossible using the crystallographic data obtained. The modeled guests are however in accordance with NMR spectroscopic data and Mass spectrometric data. Additionally, the macromolecular refinement methods employed proved to be sufficiently robust even in this very delicate case. To verify the obtained models, omit map were calculated for both structures, by omitting all atoms of the inner guest from the structure factor calculation. Omit maps in figure 10 and 11 for both structures show a good fit of the with the four symmetry equivalent positions of each guest.

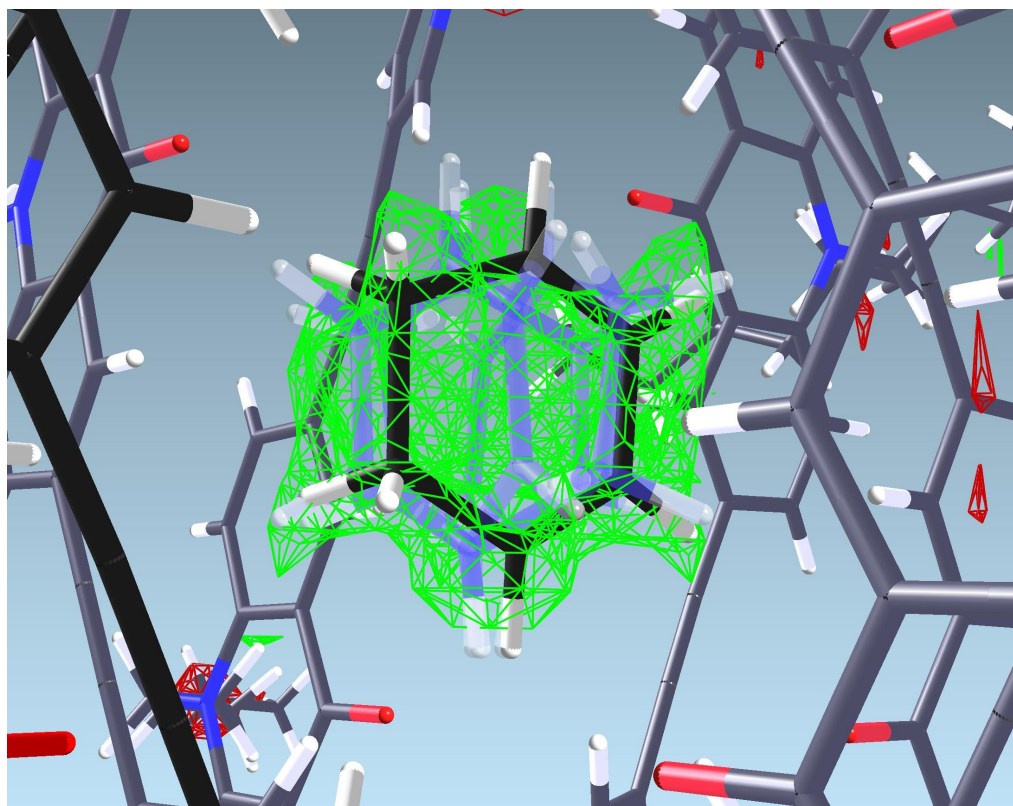


Figure S21: Omit map (in green) for encapsulated educt at $0.4 \text{ e}/\text{\AA}^3$ showing good fit of the modelled guest and its transparent symmetry equivalents on fourfold axis.

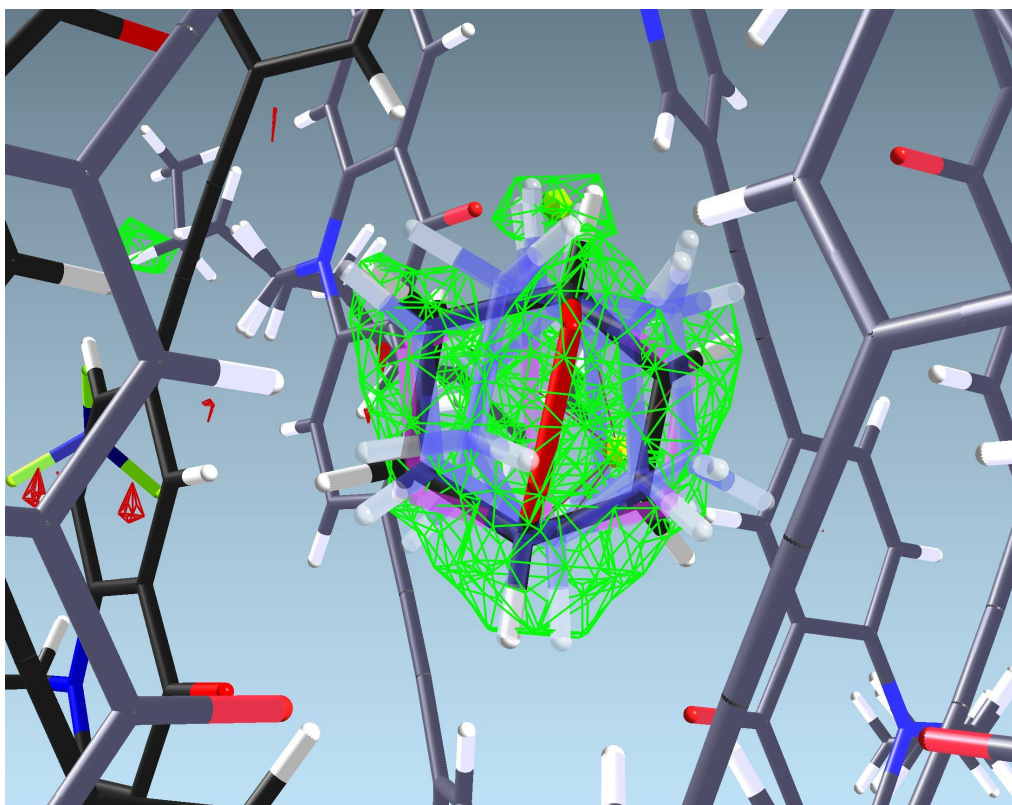


Figure S22. Omit map (in green) for encapsulated oxygen adduct at $0.6 \text{ e}/\text{\AA}^3$ showing good fit of the modelled guest and its transparent symmetry equivalents on fourfold axis.

References

- 1 S. Löffler, J. Lübben, L. Krause, D. Stalke, B. Dittrich and G. H. Clever, *J. Am. Chem. Soc.*, **2015**, *137*, 1060-1063.
- 2 W. M. Bloch Y. Abe, J. J. Holstein, C. M. Wandtke, B. Dittrich, G. H. Clever, *J. Am. Chem. Soc.* **2016**, *138*, 13750-13755.
- 3 R. Nesper, P. S. Pregosin, K. Puentener, M. Woerle *Helv. Chim. Acta* **1993**, *76*, 2239-2249.
- 4 F. Neese, *F. Wires Comput. Mol. Sci.* **2011**, *2*, 73-78.
- 5 J. G. Brandenburg, C. Bannwarth, A. Hansen, S. Grimme *J. Chem. Phys.* **2018**, *148*, 064104.
- 6 A. Burkhardt, T. Pakendorf, B. Reime, J. Meyer, P. Fischer, N. Stübe, S. Panneerselvam, O. Lorbeer, K. Stachnik, M. Warmer, P. Rödiger, D. Görries, A. Meents, *Europ. Phys. J. Plus* **2016**, *131*, 56.
- 7 W. Kabsch, *Acta Cryst. Sect. D – Biol. Cryst.* **2010**, *66*, 125-132.
- 8 G. M. Sheldrick, *Acta Cryst. Sect. A – Found. Cryst.* **2015**, *71*, 3-8.
- 9 G. M. Sheldrick, *Acta Cryst. Sect. C – Struct. Chem.* **2015**, *71*, 3-8.
- 10 C. B. Hübschle, G. M. Sheldrick, B. Dittrich, *J. Appl. Cryst.* **2011**, *44*, 1281-1284.
- 11 A. L. Spek, *Acta Cryst. Sect. C – Struct. Chem.* **2015**, *71*, 9-18.
- 12 A. L. Spek, *Acta Cryst. Sect. D – Biol. Cryst.* **2009**, *65*, 148-155.
- 13 A. Thorn, B. Dittrich, G. M. Sheldrick, *Acta Cryst. Sect. A – Found. Cryst.* **2012**, *68*, 448-451.